Space Sci Rev
DOI 10.1007/s11214-015-0139-x

The *Mars Atmosphere and Volatile Evolution* (*MAVEN*) Mission

B.M. Jakosky[1] · R.P. Lin[2] · J.M. Grebowsky[3] · J.G. Luhmann[2] · D.F. Mitchell[3] · G. Beutelschies[4] · T. Priser[4] · M. Acuna[3] · L. Andersson[1] · D. Baird[5] · D. Baker[1] · R. Bartlett[3] · M. Benna[3] · S. Bougher[6] · D. Brain[1] · D. Carson[3] · S. Cauffman[3] · P. Chamberlin[3] · J.-Y. Chaufray[7] · O. Cheatom[3] · J. Clarke[8] · J. Connerney[3] · T. Cravens[9] · D. Curtis[2] · G. Delory[2] · S. Demcak[10] · A. DeWolfe[1] · F. Eparvier[1] · R. Ergun[1] · A. Eriksson[11] · J. Espley[3] · X. Fang[1] · D. Folta[3] · J. Fox[12] · C. Gomez-Rosa[3] · S. Habenicht[4] · J. Halekas[2,13] · G. Holsclaw[1] · M. Houghton[3] · R. Howard[3] · M. Jarosz[3] · N. Jedrich[3] · M. Johnson[4] · W. Kasprzak[3] · M. Kelley[1] · T. King[3] · M. Lankton[1] · D. Larson[2] · F. Leblanc[14] · F. Lefevre[14] · R. Lillis[2] · P. Mahaffy[3] · C. Mazelle[15] · W. McClintock[1] · J. McFadden[2] · D.L. Mitchell[2] · F. Montmessin[14] · J. Morrissey[3] · W. Peterson[1] · W. Possel[1] · J.-A. Sauvaud[15] · N. Schneider[1] · W. Sidney[4] · S. Sparacino[3] · A.I.F. Stewart[1] · R. Tolson[16] · D. Toublanc[15] · C. Waters[4] · T. Woods[1] · R. Yelle[17] · R. Zurek[10]

Received: 13 September 2014 / Accepted: 13 February 2015

✉ B.M. Jakosky
Bruce.Jakosky@lasp.colorado.edu

1 Laboratory for Atmospheric and Space Physics, Univ. of Colorado, Boulder, CO, USA

2 Space Sciences Laboratory, U.C. Berkeley, Berkeley, CA, USA

3 NASA/GSFC, Greenbelt, MD, USA

4 Lockheed Martin Corp., Littleton, CO, USA

5 NASA/JSC, Houston, TX, USA

6 U. Michigan, Ann Arbor, MI, USA

7 LMD/CNRS, Paris, France

8 Boston Univ., Boston, MA, USA

9 U. Kansas, Lawrence, KS, USA

10 NASA/JPL, Pasadena, CA, USA

11 Swedish Inst. Space Phys., Uppsala, Sweden

12 Wright State Univ., Dayton, OH, USA

13 *Present address:* Univ. of Iowa, Iowa City, IA, USA

14 LATMOS/CNRS, Paris, France

15 IRAP, Toulouse, France

Published online: 09 April 2015

Abstract The MAVEN spacecraft launched in November 2013, arrived at Mars in September 2014, and completed commissioning and began its one-Earth-year primary science mission in November 2014. The orbiter's science objectives are to explore the interactions of the Sun and the solar wind with the Mars magnetosphere and upper atmosphere, to determine the structure of the upper atmosphere and ionosphere and the processes controlling it, to determine the escape rates from the upper atmosphere to space at the present epoch, and to measure properties that allow us to extrapolate these escape rates into the past to determine the total loss of atmospheric gas to space through time. These results will allow us to determine the importance of loss to space in changing the Mars climate and atmosphere through time, thereby providing important boundary conditions on the history of the habitability of Mars. The MAVEN spacecraft contains eight science instruments (with nine sensors) that measure the energy and particle input from the Sun into the Mars upper atmosphere, the response of the upper atmosphere to that input, and the resulting escape of gas to space. In addition, it contains an Electra relay that will allow it to relay commands and data between spacecraft on the surface and Earth.

Keywords Mars · Atmosphere · Solar-wind interactions · MAVEN

Acronym List (generally not including abbreviations or units)

ACC	Accelerometer
ACS	Attitude Control System
APP	Articulated Payload Platform
b.y.	billion years
b.y.a.	billion years ago
CME	Coronal Mass Ejection
DSMC	Direct Simulation Monte Carlo
EUV	Extreme Ultraviolet light
EUV	Extreme Ultraviolet sensor on the LPW instrument
eV	Electron Volts
GCM	General Circulation Model
GSFC	Goddard Space Flight Center
HGA	High-Gain Antenna
IMF	Interplanetary Magnetic Field
IUVS	Imaging Ultraviolet Spectrograph
LGA	Low-Gain Antenna
LMD	Laboratoire de Météorologie Dynamique
LPW	Langmuir Probe and Waves instrument
MAG	Magnetometer
MAVEN	Mars Atmosphere and Volatile Evolution (Mission)
MGS	Mars Global Surveyor
MHD	Magnetohydrodynamic
MLI	Multi-Layer Insulation
MOI	Mars Orbit Insertion
MPB	Magnetic Pile-up Boundary
MSL	Mars Science Laboratory
NASA	National Aeronautics and Space Administration

[16] National Institute of Aerospace, Hampton, VA, USA

[17] Univ. of Arizona, Tucson, AZ, USA

NASCAP	NASA/Air Force Spacecraft Charging Analysis Program
NGIMS	Neutral Gas and Ion Mass Spectrometer
OTM	Orbital Trim Maneuver
PTE	Periapsis Timing Estimator
RWA	Reaction Wheel Assembly
SA	Solar Arrays
SEP	Solar Energetic Particle instrument
SEPs	Solar Energetic Particles
SEU	Single-Event Upset
SSL	Space Science Laboratory
STATIC	Suprathermal and Thermal Ion Composition instrument
SWEA	Solar-Wind Electron Analyzer
SWIA	Solar-Wind Ion Analyzer
TCM	Trajectory Correction Maneuver
TWTA	Traveling Wave Tube Assembly
UHF	Ultra-high frequency
3D	Three dimensional

1 Introduction

The Mars Atmosphere and Volatile Evolution (MAVEN) mission was launched in November 2013 and arrived at Mars in September 2014. It is the second Scout-class spacecraft mission to Mars selected by NASA. It's emphasis is on studying the upper atmosphere of Mars, its interactions with the Sun and the solar wind, and the resulting loss of gas from the top of the atmosphere to space. The goal is to understand the role that loss to space has played in the climate change that is inferred to have occurred over time on Mars. As such, MAVEN is exploring the history of the habitability of Mars by microbes, and it connects up with other recent missions that have tried to understand the history of water and the habitability of the planet at and near the surface.

MAVEN is a Principal-Investigator-led mission, developed in collaboration with NASA's Goddard Space Flight Center as the management partner. The key institutions involved in MAVEN are listed in Table 1.

MAVEN was proposed in response to the 2006 Announcement of Opportunity for Mars Scout missions. In anticipation of that call, the original discussion of formulating the MAVEN mission concept and developing the team goes back to Fall 2003. MAVEN was selected to carry out a competitive Phase A study in 2007, and was selected for development for flight in 2008. The key milestones during the subsequent development for flight are listed in Table 2.

In this paper, we describe the science background and objectives, the science instruments, the spacecraft, the mission plan, data products and availability, and our approach to science closure. Each of the science instruments and the science closure are described in other papers in Space Science Reviews.

2 Science Background and Objectives

2.1 Evidence for Climate Change and Atmospheric Loss on Mars

There is abundant evidence from previous spacecraft missions that the climate on Mars has changed over time and that at least some of the atmospheric gas has been lost to space. As

Table 1 Institutional partners in MAVEN

Institution	Role on MAVEN
University of Colorado at Boulder, Laboratory for Atmospheric and Space Physics	P.I. institution, two science instruments, science-team membership, science operations, science data center, lead for Education and Public Outreach
NASA Goddard Space Flight Center	Project management, mission management, two science instruments, science-team membership, independent technical authority
Lockheed Martin	Spacecraft design and fabrication, integration and testing, mission operations
University of California at Berkeley, Space Sciences Laboratory	Deputy P.I. institution, four science instruments, science-team membership, education and public outreach
NASA Jet Propulsion Laboratory	Mars Program Office, Electra communications relay, navigation, Deep Space Network, science-team membership
IRAP	SWEA sensor, science-team membership
U. Arizona, U. Kansas, Wright State U., CNRS, N.C. State U., U. Michigan, Swedish Inst. Space Phys., NASA/JSC	Science-team membership

Table 2 Key milestones during MAVEN development for flight and early mission activities

Date	Event
January 2007	Selection for Phase A study
September 2008	Selection for development for flight
July 2010	Preliminary Design Review
July 2011	Critical Design Review
18 Nov.–7 Dec. 2013	Launch period; launch occurred on 18 November
21 Sept. 2014	Mars orbit insertion (MOI)
19 Oct. 2014	Close approach of Comet Siding Spring to Mars
16 Nov. 2014	Completion of spacecraft commissioning, start of one-Earth-year primary science mission
15 Nov. 2015	Planned completion of primary mission
16 Nov. 2015	Anticipated start of extended science and relay mission

the MAVEN science objectives were developed in direct response to these observations, we briefly summarize them here.

Geological and Geochemical Evidence Features thought to be indicative of the long-standing presence of liquid water on early Mars are observed (e.g., Carr 1996). Such features are not seen on more-recent surfaces, indicating that something about the Martian environment changed with time. The observations take two forms—morphological features and mineralogical features.

Morphological features include the valley networks and crater lakes. Valley networks are dendritic systems of valleys that appear to have formed from runoff of liquid water over long periods of time (Carr 1996; Hoke et al. 2011). They occur almost exclusively

on surfaces older than about 3.5 b.y. old (Fassett and Head 2008; Hoke and Hynek 2009). Many enclosed basins such as impact craters have features suggesting that they had standing bodies of water within them—crater lakes. Many of these show channels entering them that were capable of supplying water or leaving them and able to provide drainage. In addition, impact craters smaller than about 10–15 km diameter have been removed from the ancient surfaces, and remaining craters have been heavily degraded. Many are incised with spur-and-gully topography typical of erosion by liquid water. The best explanation is the occurrence of a major erosional event that ended approximately 3.7 b.y.a. (billion years ago), with the detailed features suggesting erosion by liquid water.

At smaller scales, features observed by the Opportunity rover are indicative of relatively shallow running water at the surface (e.g., Squyres et al. 2004). Of special note are the deposits showing "festooned layering" that are uniquely associated with shallow running water. Minerals are present on the surface that require the presence of liquid water in order to form. As observed from orbit, these include hematite, sulfates, and clays (Bibring 2006). These same minerals are seen at much smaller scales from the surface, in geometries relative to the small-scale morphological features that are consistent with their having been formed by liquid water.

Liquid water is not stable at the surface today, due to the low atmospheric pressure and the low temperatures (e.g., Jakosky and Haberle 1992). Although liquid water can occur as a transient feature, it would either freeze relatively quickly or evaporate (or sublime after freezing) into the atmosphere. It is not thought possible that it could survive long enough, or be stable enough, to produce many of the water-related features.

In general, these water-related features occur on older surfaces, dating back to before 3.7 b.y.a. The leading explanation for producing these features is the occurrence of a different climate during the earlier periods on Mars, with temperatures being warmer and water being more abundant or more available than today (e.g., Pollack et al. 1987). At the same time, the sun was an estimated 30 % dimmer in its total output than it is today, exacerbating the problem of getting sufficiently warm temperatures to allow liquid water. The best explanation for the warmer temperatures is the presence of additional greenhouse gases that would have heated the atmosphere above its equilibrium temperature. Of the plausible greenhouse gases, CO_2 is the leading candidate due to its stability and its likely abundance on the planet. Although models of the greenhouse warming have not yet satisfactorily produced conditions capable of sustaining liquid water for long periods of time (Kasting 1991), recent developments in coupling greenhouse warming with 3D atmospheric circulation models or including outgassed atmospheric hydrogen are very promising (Urata and Toon 2013; Ramirez et al. 2014).

(There also are water-related geomorphological features that do not require a climate that is different from the present-day environment. These include the large-scale flood channels produced by catastrophic release of water from the subsurface, and small-scale gullies. Each of these features can form in the present environment, given that water can survive as a liquid for the relatively short time required for these features to carve them (Baker 1982; Malin and Edgett 2003).)

Loss to Space A number of observations suggest that loss of atmospheric gases to space has occurred through time and, in fact, is ongoing today. These include measurements of the isotopes of the noble gases and light stable gases, direct observations of gas in near-Mars space that has been removed from the atmosphere, and inferences of the enhanced loss that accompanied solar-storm events at Mars.

Processes that can remove gas from the upper atmosphere to space typically differentiate between their isotopes. This occurs for two reasons. First, the loss processes for some

Table 3 Isotope ratios as observed in the Martian atmosphere. All show an enrichment of the heavier isotope relative to terrestrial values. Mars meteorite values taken from compilation in Jakosky and Jones (1994); MSL SAM results taken from Mahaffy et al. (2013) and Webster et al. (2013)

Isotope ratio	Measured value	Source
D/H	5 × terrestrial	Martian meteorites
$^{38}Ar/^{36}Ar$	1.3 × terrestrial	MSL SAM
$^{13}C/^{12}C$	1.05 × terrestrial	MSL SAM
$^{15}N/^{14}N$	1.7 × terrestrial	MSL SAM
$^{18}O/^{16}O$	1.05 × terrestrial	MSL SAM

gases differentiate between mass, so that the lighter isotopes have an easier time escaping than do the heavier isotopes. This is the case for H relative to D, and for ^{15}N relative to ^{14}N for removal via photochemical processes (Yung et al. 1988; McElroy and Yung 1976). Second, for both these gases and for the other gases, separation by mass occurs at high altitudes. Below the homopause, around 120 km above the surface, the atmosphere is well mixed. Above this altitude, mixing is not as rapid as gravitational separation, and each gas will develop its own independent scale height based on its mass. Lighter gases have larger scale heights, so that the ratio of lighter to heavier gases increases at higher altitudes. The atmosphere above the exobase altitude can be removed to space, for example via stripping of the gas by the solar wind. As the lighter gases are enriched at these altitudes relative to the heavier gases, they are preferentially removed. The now-depleted gas gets mixed back into the full atmosphere, leaving the gas that remains behind enriched in the heavier gases. This process is especially important for the isotope ratios, and can affect the ratio of the climate-related gases in D/H, $^{13}C/^{12}C$, $^{15}N/^{14}N$, and $^{18}O/^{16}O$ (McElroy and Yung 1976; Jakosky et al. 1994). Importantly, it also can affect the isotope ratios in the noble gases. The most important of these is the ratio of $^{38}Ar/^{36}Ar$, because the ratio can be changed only by loss to space (Jakosky et al. 1994).

The observed isotope ratios of some key gases are shown in Table 3. Observations come from a variety of direct and indirect sources, including direct measurement in the atmosphere from the *Viking* landers and the *Mars Science Laboratory* (*MSL*) rover, and gas trapped in the Martian meteorites that come from Mars and are collected on Earth. Two values are key here. The ratio of D/H is approximately five times the terrestrial value, and is well outside the entire range of values represented in all meteorites (Owen et al. 1988). And the ratio of $^{38}Ar/^{36}Ar$ is some 20–30 % greater than the terrestrial value. The enrichment of the heavier isotope in each of these cases can be produced only by loss of a substantial fraction of the gas from the atmosphere to space over time. Making some simple assumptions on how loss occurs, the D/H ratio requires loss of approximately 90 % of the H to space. As the source of the H is water, loss of 90 % of the water on Mars is inferred to have occurred. The $^{38}Ar/^{36}Ar$ enrichment requires loss of 50–90 % of the atmospheric argon, depending on assumptions regarding the loss processes (Jakosky et al. 1994; Jakosky and Jones 1994).

In addition to the loss inferred from the isotope ratios, direct observations show that gas can be removed to space. In particular, observations from the *Phobos* and *Mars Express* spacecraft have detected ions in near-Mars space that have been removed from the atmosphere and are being carried away by the solar wind. For example, Fig. 1 shows measurements of energetic ions made from the *Mars Express* ASPERA instrument, showing ions that are in the process of being removed from the atmosphere (Lundin et al. 1989; Barabash et al. 2007). These measurements provide direct evidence for loss of ions from the

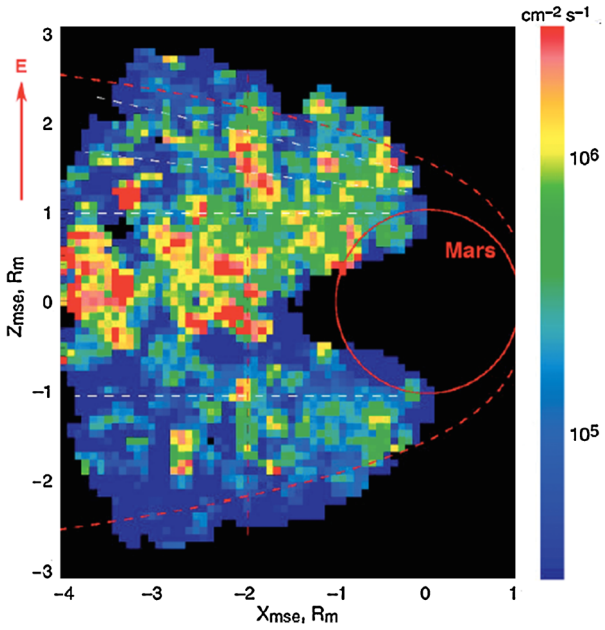

Fig. 1 Compilation of measurements from the *Mars Express* spacecraft that show ions that have been stripped away from the Mars upper atmosphere and carried tailward by the solar wind. *Dashed lines* represent the bowshock, magnetic pile-up boundary, and shadow/wake. From Barabash et al. (2007)

atmosphere to space today. While the total rate of loss to space inferred from these observations is relatively low at the present epoch and under typical solar conditions, the rate is thought to have been greater in the past when the solar activity was expected to have been greater.

In summary, there are strong observational reasons to think that loss of atmospheric gas to space has occurred, both recently and over time. The total loss inferred is likely to have been a significant fraction of the atmosphere that was present 3.5–4.0 b.y.a., and appears to be a viable mechanism for the subsequent changes in climate inferred to have occurred based on the geological and geochemical observations.

2.2 Brief Summary of Mechanisms for Atmospheric Loss

Multiple mechanisms have been proposed by which gas can be removed or lost from the Martian atmosphere to space. The lack of comprehensive measurements at Mars means that most of the processes are based on extrapolation from observations at Earth, Venus, and comets, where interactions with the solar wind have been observed in detail. Brief descriptions of the processes and of the observations that can allow us to infer their efficacy follow. To aid in this discussion, Fig. 2 shows an overview of the different regions of the atmosphere.

Jeans Escape Jeans escape rates can be determined from knowledge of the neutral composition and temperature at and near the exobase, as was done using *Mariner* 9 and *Mars Express* ultraviolet observations (Anderson and Hord 1971; Chaufray et al. 2008; Chaffin et al. 2014). With neutral atoms having a temperature of ~ 250 K (0.02 eV for H, compared to ~ 0.1 eV escape energy) at the exobase, Jeans escape is significant for the loss of H, deuterium (D), and He. The differential escape of H and D due to their different masses will increase the D/H ratio of the remaining gas (Yung et al. 1988).

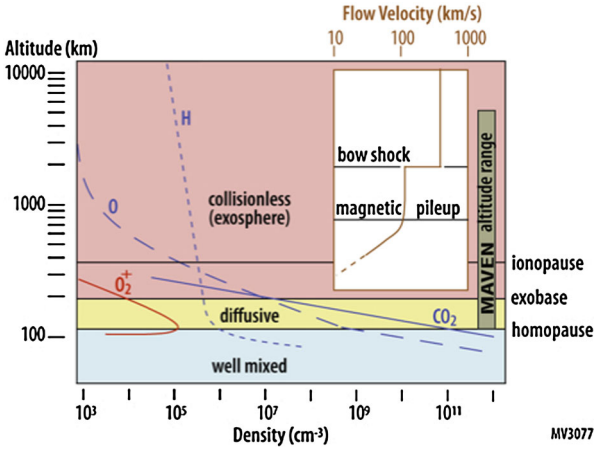

Fig. 2 Overview of the different regions of the Martian upper atmosphere and of its interactions with the solar wind. The boundaries between the well-mixed lower atmosphere, the diffusively controlled upper atmosphere, and the collisionless exosphere are shown. Nominal profiles of H and O atoms in the extended corona, and of O_2^+ ions in the ionosphere are shown for reference. The *insert* shows nominal altitudes in the upstream direction for the bow shock and magnetic pile-up boundary as the solar wind impinges on the planet, and a nominal profile of the solar-wind flow velocity as a function of altitude

Photochemical Loss Photochemical processes in which exothermic reactions result in velocities greater than thermal velocities can result in escape of O, N, and C. For example, the dissociative recombination reaction of the dominant ionosphere species O_2^+ with electrons can produce two energetic O atoms with speeds of ~ 6.5 km/sec, exceeding the 5 km/s escape speed at Mars; a similar process occurs for the production of energetic atoms of O, N, and C from CO_2^+, N_2^+, and CO^+, respectively. Photodissociation and photoelectron impact dissociation of the molecular species also produce non-thermal atoms that can escape (McElroy 1972). Ionospheric electrons can affect the photochemistry in two ways. Some of the reaction rates depend on the electron temperature, and the more-energetic photoelectrons (10–60 eV or more) are an additional source of ionization and dissociation. The observed enrichment of $^{15}N/^{14}N$ in the Martian atmosphere is a strong (albeit not unique) indicator that this process has operated (McElroy et al. 1977). The total exospheric loss rate from all processes is ultimately limited by the maximum rate at which dynamical and photochemical processes can supply atoms to the exobase region and corona (Fox 1997).

Ion Loss Once ionized, several processes can transfer energy from the solar wind to planetary ions and lead to heating, acceleration, and escape. Unlike neutrals, ions do not need to be created with escape velocity but can be accelerated subsequently. Ion loss mechanisms fall into three main categories: *ion pickup, ion bulk escape*, and *ion outflow*. The first two occur in the absence of a strong planetary magnetic field, as at Venus, where the upper atmosphere and ionosphere are exposed directly to the solar wind. The third can occur in the presence of planetary magnetic fields, as at Earth. Both regimes occur at Mars, where there is no internal dipole magnetic field but there are strong crustal magnetic fields over portions of the planet (Acuña et al. 1999). Because of the lack of comprehensive measurements at Mars, we do not understand ion loss rates and the processes that control them, which loss processes dominate, or how they respond to atmospheric and solar variability.

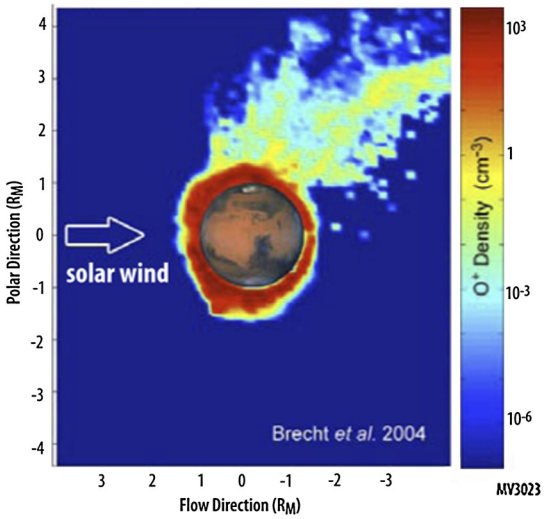

Fig. 3 Results of a numerical model of interaction of the impinging solar wind with the Mars environment. The *colors* represent the O^+ density, and clearly show ionospheric plasma being picked up by the solar wind and carried downstream over the pole. While the details of the interactions vary among different modelers, the general nature of the interaction and of solar-wind stripping of ions from the ionosphere are common to all models. From Brecht et al. (2004)

Pickup Ions and Atmospheric Sputtering Neutrals that are ionized in a magnetized plasma that is moving with velocity **v**, such as the solar wind or the magnetosheath plasma (shocked solar wind) that flows around Mars, or ions that find their way into regions affected by solar-wind-induced fields, will be accelerated by the $\mathbf{v} \times \mathbf{B}$ electric field and gyrate around magnetic field lines. At high altitudes, their trajectories can be large helices (up to $\sim$ 30,000 km radius for O^+). These pickup ions come predominantly from the Sun-facing hemisphere of Mars, and have velocities ranging from zero to twice the plasma flow speed, $\sim$ 350–700 km/s for the solar wind, and corresponding pickup ion energies ranging to greater than 10 keV (Fig. 2, inset). Although pickup ions can be produced anywhere in the solar-wind interaction region, the dominant source is below the Magnetic Pileup Boundary (MPB), at altitudes $<$ 800 km where the neutral density is higher and the stagnating solar wind is still moving fast enough to give pickup ions escape velocity (e.g., Jin et al. 2001). Since the solar-wind magnetic field typically penetrates down to the exobase region at Mars, the pickup process can operate at altitudes where the bulk flow velocity is less than 10 km/s, with corresponding pickup energies for O^+ of tens of eV. Most pickup ions are accelerated over the planet's poles (for a typical solar-wind magnetic field) and can be lost down the wake (Fig. 3). This low-energy population almost certainly dominates the overall pickup loss, but has never been measured at Mars (e.g., Curry et al. 2013).

Some pickup ions have trajectories that impact the atmosphere with sufficient energy to impart escape velocity to exospheric neutrals by collisions, a process termed atmospheric sputtering (Luhmann et al. 1992; Johnson 1994). The impacts also cause additional heating and ionization near the exobase, which in turn enhances the pickup-ion population, creating a positive feedback mechanism (Johnson and Luhmann 1998). Model calculations (Leblanc and Johnson 2002; Fang et al. 2013) suggest that sputtering should occur at the present epoch at a low level compared to other ion loss processes, but the process could have been more important for both atmospheric loss and neutral atmospheric heating during disturbed periods like those believed to have been prevalent earlier in solar system history. Estimates of the present-day O^+ escape rate based on *Phobos 2* data (e.g., Lundin et al. 1989; Luhmann and Kozyra 1991; Luhmann et al. 1992) do not account for crustal magnetic fields that can partly shield the atmosphere from the solar wind (Mitchell et al. 2001; Brain et al. 2003). In addition, the equatorial orbit of *Phobos 2* missed part of the main pickup-ion flux at polar

latitudes. In contrast, *Mars Express* has observed planetary ions with pickup energies, at altitudes well below 800 km altitude (Lundin et al. 2006a, 2006b). However, the magnetic field was not measured by *Mars Express*, severely hampering the ability to understand how ions are being accelerated away from the planet. In addition, many of the external drivers of ion loss were either not measured by *Mars Express* or were indirectly inferred via proxy measurements. Thus, there remains a major gap in understanding the process that drives the potentially key pickup-ion precipitation and loss.

Solar Energetic Particles (SEPs) are accelerated by solar flares and associated fast Coronal Mass Ejections (CMEs) to much higher energies (10 s of keV to $>\sim$ 100 s of MeV) than pickup ions. They may also produce sputtering, heating and ionization effects similar to those by pickup ions, but extending much deeper into the atmosphere (Leblanc et al. 2002). SEP events typically start with an impulsive, $\sim$ 10–100 minute duration, solar flare EUV and X-ray burst. The fastest (relativistic) SEPs arrive within $\sim$ 1 hour, followed by slower SEPs (down to tens of keV). About 1–2 days later, the CME arrives with high speed, greater than the $\sim$ 1000 km/s solar wind, and strong magnetic fields. How these transient inputs to the Martian atmosphere drive losses is not known. During the 28 October 2003 SEP event, the largest of the last solar cycle, *MGS* observations showed that the neutral density of Mars' upper atmosphere may have decreased by nearly an order of magnitude for $\sim$ 24 hours before recovering (Lillis et al. 2005). During the passage of the storm the solar wind interaction region was compressed (Crider et al. 2005), and plasma waves associated with planetary ions are observed on the nightside (Espley 2005), both suggesting that atmospheric escape rates increased. Futaana et al. (2008) and Edberg et al. (2010) have reported evidence of enhanced atmospheric ion escape at disturbed times, but these results are based on incomplete information given the lack of magnetic field measurements and SEP measurements on *Mars Express*. The cumulative losses from such events over time may have been very significant, especially in the early active phase of the Sun (lasting $\sim$ 0.5–1 b.y.) which was characterized by continuous flare events with a particle and radiation environment several hundred times more intense than at present (Lammer et al. 2003).

Ion Bulk Escape Momentum transfer from the impinging solar wind may strip off coherent blobs of plasma from the ionosphere. Such detached "clouds" of ions and electrons would be carried downstream by the solar wind and lost, analogous to the detached tail of a comet. Although few measurements are available at Mars, similar processes have been observed at Venus. There, thermal ion measurements made from *Pioneer Venus* revealed a complex morphology of the ionosphere upper boundary near the Venus terminator and in the wake, consisting of waves, streamers, and detached ionospheric "clouds" (Brace et al. 1982), which might have been generated by Kelvin–Helmholtz (K–H) instability (Elphic and Ershkovich 1984) or by magnetic tension ("slingshot") related to the draped solar-wind magnetic fields. At Mars, the presence of crustal magnetic fields interacting with shocked solar wind plasma makes possible additional bulk escape mechanisms, including magnetic reconnection (Eastwood et al. 2008) and plasmoid-type structures (Brain et al. 2010). In addition, nightside ions could be accelerated downwind by solar-wind-induced electric fields, leading to loss (Grebowsky and Curtis 1981). At Mars, measurements suggest the presence of similar streamers and clouds (Cloutier et al. 1999; Mitchell et al. 2001; Dubinin et al. 2006), although available observations do not distinguish between escaping clouds or ionospheric irregularities. Therefore, the efficacy of bulk escape mechanisms at Mars is unknown.

Ion Outflow At high latitudes on Earth there is significant outflow of planetary ions to space on "open" magnetic field lines that connect to interplanetary field lines. Outflow is driven by outward directed electric fields and by ion heating. Electric fields are always present on open field lines because thermal electrons are not gravitationally bound and can escape; the resulting charge separation sets up an electric field that accelerates ions outward to form a *polar wind* (André and Yau 1997; Ganguli 1996). The large-scale current system driven by the solar wind as it flows past Earth's magnetosphere can create much stronger electric fields in auroral regions, with correspondingly more intense ion outflows (Paschmann et al. 2003). There also can be intense heating of ions at low altitude, caused by resistive dissipation of the solar wind/magnetosheath electric field that maps down into the lower ionosphere. Such resistive heating produces a thermal upwelling of ions. Waves generated by the interaction of the solar wind with Mars have been detected by *MGS* (Espley 2004). These waves can propagate down to the ionosphere and heat O^+ ions perpendicular to the magnetic field by resonant wave interaction; the O^+ ions can be subsequently accelerated outward by the mirror force of the diverging magnetic field. On Mars, the loops formed by remnant crustal magnetic fields will connect at times with the solar-wind interplanetary magnetic field (IMF) lines, forming cusps and open magnetic field lines, smaller but otherwise analogous to Earth's features (Krymskii et al. 2002). Evidence for outward ion acceleration and outflow at Mars is provided by auroral UV emissions (Bertaux et al. 2005), energetic peaked aurora-like electron precipitation (Brain et al. 2006; Lundin et al. 2006b) observed in cusp regions adjacent to Martian minimagnetospheres, and the presence of keV ions in the magnetotail (Fedorov et al. 2006; Dubinin et al. 1993, 2006). It is difficult to assess the role that crustal magnetic fields play in ion outflow with existing data. While calculations show potentially significant loss via ion outflow (Ergun et al. 2006; Andersson et al. 2010), it is impossible to assess the actual magnitude or importance of this loss relative to other processes without additional measurements.

2.3 MAVEN Science Objectives

In summary, there is abundant observational and theoretical evidence to support the idea that escape of gas from the Martian atmosphere to space may have been a significant process that, over time, may have contributed substantially to the change in climate inferred from the geological and geochemical observations. Other potential processes for removal of gas from the atmosphere would include formation of carbon- or water-bearing minerals in the crust from atmospheric CO_2 and H_2O and percolation of water from the atmosphere into the crust. At present, indications are that these latter processes are not, in and of themselves, of sufficient magnitude to be able to explain the climate change. At a minimum, the total magnitude of loss to space, and the relative importance of the different processes, is not known today.

With this context in mind, the MAVEN mission was designed to explore the role of loss of atmospheric gas to space. Our high-level science objectives are:

– *Measure the composition and structure of the upper atmosphere and ionosphere today, and determine the processes responsible for controlling them.* We will determine the range of properties, and how they depend on the geographical location and external conditions (and the underlying driving processes such as interaction with the remnant magnetized regions of the Martian crust). By determining the controlling processes, we will be able to extrapolate back in time to understand what the upper atmosphere would have looked like under the different boundary conditions of the solar EUV and the solar wind that occurred early in solar-system history.

– *Measure the rate of loss of gas from the top of the atmosphere to space, and determine the processes responsible for controlling them*. Again, by determining the underlying processes and their ranges of variations, we can extrapolate to early epochs when conditions would have been different.
– *Determine properties and characteristics that will allow us to extrapolate backwards in time to determine the integrated loss to space over the four-billion-year history recorded in the geological record.*

Details of how we will achieve our objectives will be outlined in the section on science closure, following discussion of the instruments, observing plan, and mission plan.

3 Science Instruments and Science Team

3.1 Overall Approach

In order to achieve our objectives, we need to track the energy inputs from the Sun, and the upper-atmospheric and ionospheric response to those inputs. The energy inputs from the Sun consist of the solar EUV radiation incident on the upper atmosphere, the solar wind as it interacts with the magnetospheric obstacle around the planet and then with the ionosphere, and solar energetic particles from flares and coronal mass ejections. The response of the upper atmosphere includes the composition and structure of the upper atmosphere and ionosphere, and how these vary in response to the energetic inputs. The processes responsible for these are expected to vary spatially, in response to the varying incidence angle and orientation with regard to the magnetospheric boundaries, in response to the geographically varying magnetic field, and as driven by upper-atmospheric circulation patterns. The surface has localized regions of crust that are strongly magnetized and that drive interactions with the solar wind; in response, they produce cusp-like regions, and the interactions with the solar wind will vary depending on local orientation and ionospheric properties. The energetics of these interactions also drive escape processes, and these processes also will vary depending on the local properties and geometry.

Figure 4 shows the high-level approach to our science traceability, in which the science objectives of MAVEN drive the approach to answering the questions. This approach then drives the characteristics and requirements of the individual science instruments (this latter part of the "science traceability matrix" is not shown here).

Table 4 lists the science instruments on MAVEN. Although they integrate into the science based on the flow of energy into the system and the response of the system, they are organized into three packages based on the instrument design and accommodation onto the spacecraft. They are the Particles and Fields Package, the Remote Sensing Package, and the Mass Spectrometry instrument. Each instrument is described briefly below, and in more detail in the accompanying papers. Figure 5 shows each of the science instruments.

The LPW instrument is divided into two quasi-independent components that are integrated into a single instrument. The Langmuir Probe and Waves component analyzes the properties of the ionosphere. The EUV component monitors the EUV emissions from the Sun. Although they comprise a single instrument and are described here as such, the hardware and the science are described separately in the accompanying papers.

In addition, the spacecraft has an accelerometer (ACC) and reaction wheel assembly (RWA) on board that are used to determine the density of the upper atmosphere as we pass through it on each orbit near periapsis. Although MAVEN does not get to as low an altitude

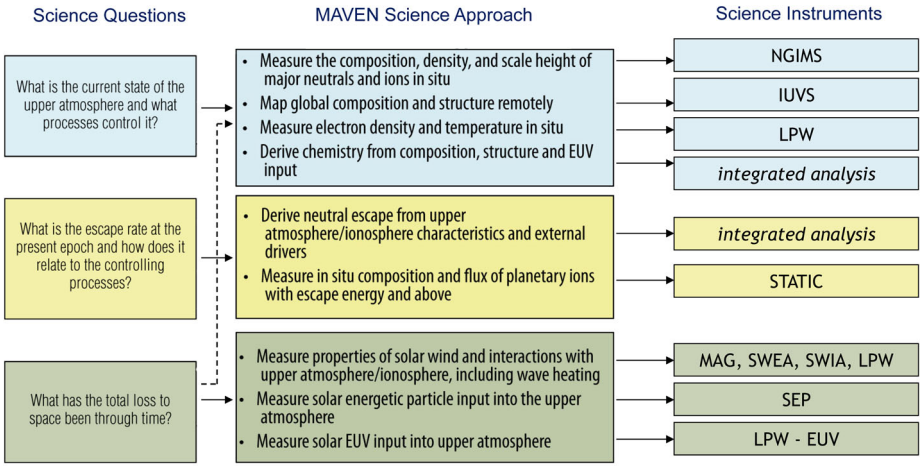

Fig. 4 Simplified traceability diagram showing how the science questions for MAVEN lead to the required measurements and then to the science instruments. The specific measurement requirements and the characteristics of the instruments are not shown. "Integrated analysis" refers to properties that are calculated from other measurements rather than directly measured

Table 4 Science packages and instruments on MAVEN

Package name	Instrument name	Abbreviation
Particles and Fields Package	Solar Wind Electron Analyzer	SWEA
	Solar Wind Ion Analyzer	SWIA
	Solar Energetic Particle instrument	SEP
	Suprathermal and Thermal Ion Composition instrument	STATIC
	Langmuir Probe and Waves (including EUV component)	LPW
	Magnetometer	MAG
Remote Sensing Package	Imaging Ultraviolet Spectrometer (with accompanying Remote Sensing Data Processing Unit)	IUVS
Mass Spectrometry instrument	Neutral Gas and Ion Mass Spectrometer	NGIMS

(and as high a density) as previous spacecraft did during aerobraking, it still gets to an altitude at which the spacecraft will sense the atmosphere. Operationally, the data from the ACC and RWA are used to adjust the periapsis timing estimator (PTE) so that spacecraft sequences and pointing relative to the ram direction are timed properly. Scientifically, these will be used to determine the density of the upper atmosphere at the altitude of the spacecraft.

The packages and instruments are described briefly below.

3.2 Remote-Sensing Package

IUVS The Imaging UltraViolet Spectrograph is a remote-sensing instrument that measures UV spectra with four observing modes: (1) limb scans near periapsis; (2) planetary mapping at two spectral resolutions; (3) coronal mapping; (4) stellar occultations. These measurements will:

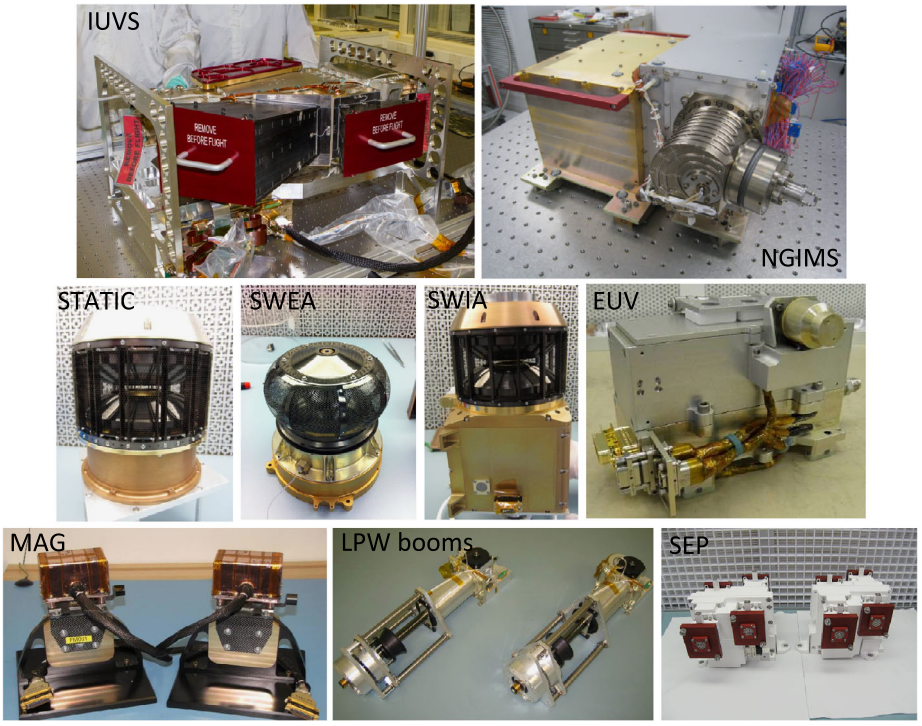

Fig. 5 MAVEN science instruments. The EUV component of the LPW is shown separately. The ACC is not shown

- Provide the composition and structure of Mars' upper atmosphere, ionosphere, and corona
- Provide the photochemical loss rates for C, N, and O
- Provide the Jeans escape rates for H, D, and He
- Provide stable-isotope ratios
- Measures CO_2 photoionization emissions as a proxy for the solar EUV flux

3.3 Particles and Fields Package

STATIC The Supra-Thermal And Thermal Ion Composition (STATIC) instrument measures the velocity distributions and mass composition of suprathermal and thermal ions. These measurements provide:

- Density profiles of major ions (H^+, He^{++}, He^+, O^+, O_2^+, CO_2^+)
- Flow velocities from < 1 to > 25 km/s
- Ion temperature from ~ 0.1 eV to > 10 eV
- Pickup ion composition and flux up to energies of 30 keV

For MAVEN's science objectives it is essential to measure loss of ions down to the escape velocity (5 km/s or ~ 2.5 eV for O^+). The STATIC instrument is optimized to measure the full velocity distribution (and composition in the major ion mass ranges), down to 0.5 eV energy (O_2^+ energy at spacecraft ram speed is 4.6 eV).

SEP The Solar Energetic Particle (SEP) instrument measures the energy spectrum and angular distribution of solar energetic electrons (30 keV–1 MeV) and ions (30 keV–12 MeV). With these measurements, SEP will:

- Determine SEP energy input as a function of altitude
- Determine SEP heating, ionization, and sputtering of the upper atmosphere
- Detect the highest energy pickup ions (> 30 to 100 s of keV)

SWIA The Solar Wind Ion Analyzer (SWIA) measures the energy and angular distributions of solar wind and magnetosheath ions. With these measurements, SWIA:

- Determines the solar wind (H^+ and He^{++}) and magnetosheath density, temperature, and bulk flow velocities around Mars
- Determines the ionization rate of neutrals from charge exchange with solar-wind ions
- Determines the pickup acceleration of newly formed ions by the $\mathbf{v} \times \mathbf{B}$ electric field
- Determines the solar wind dynamic pressure

SWEA The Solar Wind Electron Analyzer (SWEA) measures the energy and angular distributions of 5 eV to 6 keV solar wind and magnetosheath electrons and ionospheric photoelectrons. With these measurements, SWEA:

- Determines the electron impact ionization rates in all regions sampled by MAVEN
- Distinguishes the energy spectra of ionospheric primary photoelectrons, and of solar wind, magnetosheath, and magnetotail electrons to determine plasma environment
- Captures single- and double-sided ionospheric loss cones to determine magnetic topology (locations of magnetic cusps and extents of crustal magnetospheres)
- Identifies auroral ($\sim$ keV) electron populations and determines their role in ionization and dissociation processes
- Measures the primary photoelectron spectrum as a proxy for the solar EUV flux

LPW The Langmuir Probe and Waves (LPW) instrument incorporates the solar Extreme Ultraviolet (EUV) monitor. The LPW measures electron density (n_e) and temperature (T_e) and electric field waves in the Mars environment. The EUV Monitor provides additional measurements for determining the solar EUV input to the Mars atmosphere, from photodiode measurements and from the LPW photoelectron saturation current. With these measurements, LPW will:

- Identify the ionopause and detached ionospheric clouds
- Derive recombination rates
- Provide an estimate of Poynting flux into the ionosphere and ionosphere heating rates (with MAG)
- Provide proxy measurements of the solar EUV flux over the entire EUV spectrum

MAG The dual vector fluxgate magnetometer (MAG) measures the intensity and direction of the magnetic field—interplanetary, induced magnetospheric, ionospheric and crustal—in all regions traversed by MAVEN in its orbit. With these measurements, MAG will:

- Determine the morphology of the ionosphere and magnetosheath (with LPW and SWEA)
- Determine the structure and topology of the magnetic cusp regions (with SWEA)
- Determine the convection electric field (with SWIA)

3.4 Mass Spectrometry Package

NGIMS The Neutral Gas and Ion Mass Spectrometer will measure the neutral composition, isotopic ratios and scale height temperature of the major gas species (He, N, O, CO, N_2, NO, O_2, Ar, and CO_2) and thermal ions in the Martian upper atmosphere. These *in-situ* measurements will:

- Determine the variation of the neutral composition with altitude, local solar time, longitude and season from the homopause to the exobase where neutral gas can escape.
- Provide a basis for the study of thermospheric energetics, transport, circulation, and formation of the ionosphere.
- Reveal the effects of lower atmosphere meteorological effects, such as dust storms, on the composition of the upper atmosphere and exobase.

3.5 Science Team

The MAVEN science team consists of science leads, instrument teams, interdisciplinary scientists, and participating scientists. The science leads are the Principal Investigator, the Deputy Principal Investigator, and the GSFC-based Project Scientist. (Bob Lin was the Deputy Principal Investigator from the beginning of the Project in 2003 until his death in November 2012. Janet Luhmann, who was one of the science leads from the beginning, was appointed to replace him as Deputy P.I. in April, 2013.) The nine Participating Scientists were selected in Spring 2013 as the result of an open competition in order to expand the MAVEN science team and enhance the science return from the mission; upon selection, they became full members of the science team. Table 5 lists the members of the MAVEN science team.

4 Spacecraft

4.1 Spacecraft Design

The MAVEN spacecraft design is based on the mission requirements of being able to accommodate the anticipated science instruments and ensuring that they can make their observations for the required one Earth year. Individual components draw on heritage from previous Lockheed Martin spacecraft where possible, including the *Juno*, *Grail*, and *Mars Reconnaissance Orbiter* spacecraft.

The spacecraft is three-axis stabilized, with an Articulated Payload Platform (APP) that allows three instruments to be oriented in space independent of the spacecraft orientation (Fig. 6). This configuration allows those instruments that need to be pointed relative to the Sun or to the solar wind to be oriented properly, while also allowing those instruments that need to be pointed at the planet to do so. The former instruments are fixed on the spacecraft or on fixed booms, and the spacecraft is generally operated with its z-axis (running through the High-Gain Antenna) pointed toward the Sun. The two gimbals on the APP allow the instruments needing orientation relative to the planet to be properly pointed.

With this configuration, the spacecraft can have fixed solar arrays and high-gain antenna (HGA). The spacecraft and the solar arrays point at the Sun, and can be off-pointed when necessary and within the constraints imposed by power requirements. With a fixed HGA, the entire spacecraft must be pointed toward the Earth in order to allow communications. During science operations, this is done twice weekly, during 5-hour communications sessions.

Table 5 Members of the MAVEN science team

Category	Title	Name	Affiliation
Science Leads	Principal Investigator	Bruce Jakosky	University of Colorado
	Deputy P.I. (deceased)	Bob Lin	University of California at Berkeley
	Deputy P.I.	Janet Luhmann	University of California at Berkeley
	Project Scientist	Joe Grebowsky	NASA/GSFC
IUVS team	Instrument/science lead	Nick Schneider	Univ. of Colorado
	Hardware lead	Bill McClintock	Univ. of Colorado
	Co-I	Ian Stewart	Univ. of Colorado
	Co-I	John Clarke	Boston Univ.
	Co-I	Greg Holsclaw	Univ. of Colorado
	Co-I	Erik Richard	Univ. of Colorado
	Co-I	Franck Montmessin	LATMOS, CNRS
	Collaborator	Jean-Yves Chaufray	LMD-IPSL, CNRS
	Collaborator	Franck Lefevre	LATMOS, CNRS
NGIMS team	Instrument lead	Paul Mahaffy	NASA/GSFC
	Science lead	Mehdi Benna	NASA/GSFC
	Co-I	Wayne Kasprzak	NASA/GSFC
SWEA team	Instrument lead	David L. Mitchell	Univ. of California at Berkeley
	Co-I	Christian Mazelle	IRAP
	Co-I	Jean-Andre Sauvaud	IRAP
	Co-I	Dominique Toublanc	IRAP
SWIA team	Instrument lead	Jasper Halekas	Univ. of Iowa
	Co-I	Rob Lillis	Univ. of California at Berkeley
	Co-I	Davin Larson	Univ. of California at Berkeley
SEP team	Instrument lead	Davin Larson	Univ. of California at Berkeley
	Co-I	Jasper Halekas	Univ. of Iowa
STATIC team	Instrument lead	Jim McFadden	Univ. of California at Berkeley
	Co-I	Francois Leblanc	LATMOS/CNRS
LPW team	Instrument lead	Bob Ergun	Univ. of Colorado
	Science lead	Laila Andersson	Univ. of Colorado
	Co-I	Anders Eriksson	Swedish Inst. of Space Physics
	Co-I	Greg Delory	Univ. of California at Berkeley
EUV team	Instrument lead	Frank Eparvier	Univ. of Colorado
	Co-I	Phil Chamberlin	NASA/GSFC
	Co-I	Tom Woods	Univ. of Colorado
MAG team	Instrument lead	John Connerney	NASA/GSFC
	Co-I	Jared Espley	NASA/GSFC
	Instrument lead (deceased)	Mario Acuna	NASA/GSFC

Table 5 (*Continued*)

Category	Title	Name	Affiliation
Atmospheric Advisory Group	Team lead	Richard Zurek	NASA/JPL
	Co-I	Bob Tolson	Natl. Inst. Aerospace
	Co-I	Darren Baird	NASA/JSC
Interdisciplinary Scientists	Co-I	Tom Cravens	Univ. of Kansas
	Co-I	Xiaohua Fang	Univ. of Colorado
	Co-I	Jane Fox	Wright State Univ.
	Co-I	Roger Yelle	Univ. of Arizona in Tucson
	Co-I	David Brain	Univ. of Colorado
	Co-I	Dan Baker	Univ. of Colorado
	Co-I	Bill Peterson	Univ. of Colorado
	Co-I	Steve Bougher	Univ. of Michigan
	Collaborator	Andy Nagy	Univ. of Michigan
Participating Scientists	P.S.	Michael Combi	Univ. of Michigan
	P.S.	Frank Crary	Univ. of Colorado
	P.S.	Scott England	University of California at Berkeley
	P.S.	Yingjuan Ma	UCLA
	P.S.	Michael Mendillo	Boston U.
	P.S.	Pascal Rosenblatt	Royal Observatory of Belgium
	P.S.	Kanako Seki	Nagoya Univ.
	P.S.	Michael Stevens	Naval Research Lab.
	P.S.	Paul Withers	Boston U.

In addition to the HGA, we have two low-gain antennas (LGAs). Together, they provide essentially full-sky coverage. The LGAs are used to communicate with the spacecraft following launch, during Mars orbit insertion (MOI), during any entries into safe mode, and to allow communications for tracking during science operations.

There are four booms to accommodate the science instruments, as described further in the next section (see Fig. 6). MAVEN was launched with the APP folded up against the spacecraft body. On the opposite side of the spacecraft, the SWEA boom also was folded up against the body. These booms are on hinges, with releases that allowed them to swing out and lock into place. The LPW probes are on 7-m stacer booms. These booms consist of a spiral-coiled metal strip that extends upon release, much like an old-fashioned child's spiral "shooter" toy (known in some circles as a Fling Zing Chinese Yo-Yo). All four booms remained stowed until after orbit insertion, and were released during the commissioning phase of the spacecraft.

In addition, the two MAG sensors are located on small fixed booms extending out from each end of the solar arrays (SAs). By putting them at the end of the SAs, and then extending them further out on the end of so-called "diving boards", they get the maximum distance possible from the rest of the spacecraft in order to minimize spacecraft magnetic fields.

The spacecraft is built around the core structure, which encloses the hydrazine fuel tank at the center of the body (Fig. 7). The primary structure surrounding the fuel tank is built as an open structure, with four bays allowing easy access to the spacecraft components during

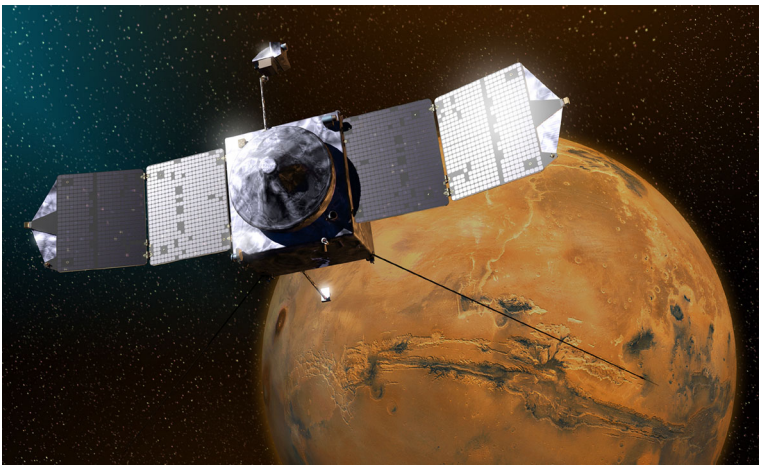

Fig. 6 Artist's conception of the MAVEN spacecraft. High-gain antenna in the middle is 2 m diameter for scale. Articulated Payload Platform (APP) is visible at the *top*; SWEA boom at *bottom center*; one of the LPW booms is visible at *lower right*. The second panel of each solar-array wing is canted for increased aerodynamic stability

Fig. 7 Early stage in assembly of the MAVEN spacecraft, showing the core structure being lowered onto the fuel tank that sits within the central core

assembly and testing (Fig. 8). Individual components were fixed at locations within the bays that would provide the proper overall center of mass both with the booms stowed in their launch configuration and then with them extended for the science phase of the mission.

The solar arrays were stowed for launch, with the on-orbit configuration requiring that they be stowed with their active solar-cell faces pointed inward. They extended immediately upon spacecraft separation from the upper stage during launch. When extended, they have a split, gull-wing configuration, and are located at the extreme $-$z end of the body. This configuration and location provides a substantial offset between the spacecraft center of mass

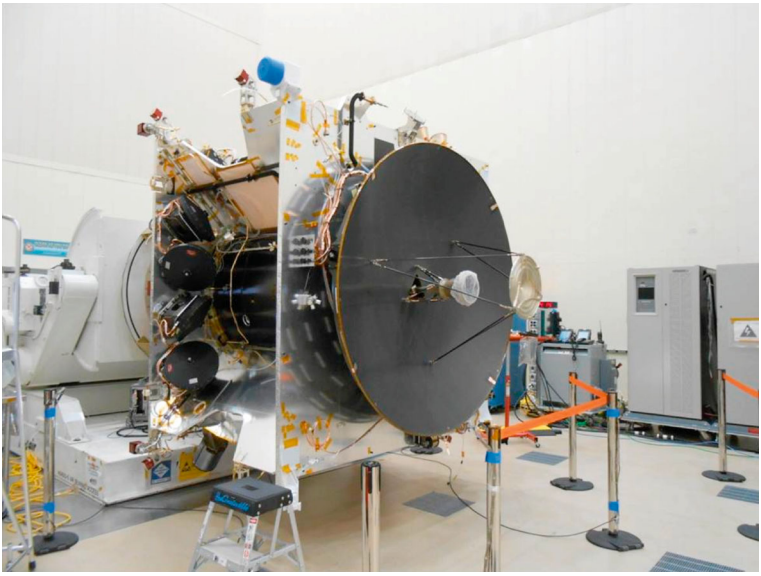

Fig. 8 Nearly completely assembled MAVEN spacecraft, showing the open-bay construction. The bay that is visible contains the four reaction wheels, oriented parallel to the four top faces of a pyramid

and the center of force during the passages through the tenuous upper atmosphere during the "deep dips". This offset provides strong aerodynamic stability, much as a shuttlecock would have a stable orientation during a game of badminton.

Spacecraft orientation is provided by either thrusters or reaction wheels. There are four reaction wheels for maximum control and redundancy. Full control and redundancy is provided by having the four wheels oriented parallel to the four top faces of a pyramid (Fig. 8). This configuration provides more control with less stress on the wheels than having them oriented along the three cardinal axes with a fourth skewed wheel, while still providing complete redundancy in case of failure of any one wheel. Attitude control during the mission is generally provided by the wheels, with thrusters used to remove angular momentum regularly to keep the wheels from spinning too fast.

The spacecraft uses its "periapsis timing estimator" (PTE) software to estimate the density of the upper atmosphere at the location of the spacecraft. The estimate is based on the known aerodynamic properties of the spacecraft and on the changes induced in the reaction wheel spin rates, and on the acceleration of the spacecraft due to drag as measured by the accelerometer. In response, the spacecraft will calculate the changes induced in its orbit and the timing of when periapsis will be reached. This information is used to adjust pointing in the instruments on the APP, in order for them to obtain their required observations. The PTE process was used previously on missions utilizing aerobraking; it can be used here because we penetrate sufficiently deeply into the upper atmosphere to sense the atmospheric drag even though MAVEN does not utilize aerobraking.

Mars orbit insertion (MOI) was carried out with six thrusters located on the back end of the spacecraft. They fired during MOI for approximately 33 minutes, putting us into a 35-hour elliptical orbit around the planet. The Trajectory Correction Maneuver (TCM) thrusters were used to adjust both periapsis and apoapsis of the orbit to get into our final mapping orbit, while Attitude Control System (ACS) thrusters control the spacecraft attitude

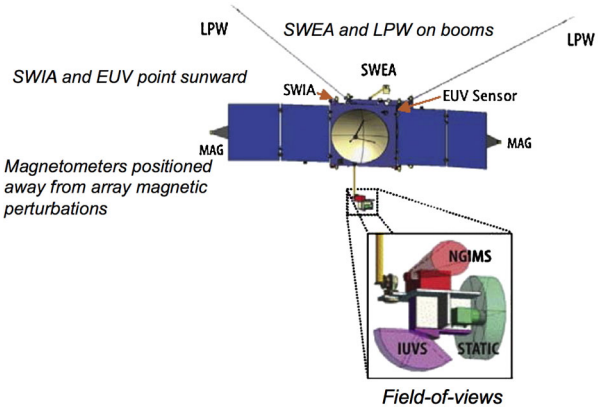

Fig. 9 Instrument accommodation. *Diagram* shows the locations of the science instruments on the body of the spacecraft and on the APP

and remove accumulated momentum from the reaction wheels. Hydrazine is used to fuel all spacecraft thrusters.

The spacecraft launched on an Atlas V-401 launch vehicle, during a 20-day launch period extending from 18 November–7 December, 2013. The original 20-day period was based on the published capability of the Atlas V launch vehicle and Centaur upper stage, and on the ability to get into orbit with the fuel that could be carried on the spacecraft. The as-built spacecraft is approximately 80 kg under its "not to exceed" mass, and the launch vehicle increased its capability as margin was released; together, these allowed a longer launch period, extending to as many as 12 days past the nominal 7 December date. Launch occurred at the first opportunity on the first day of the launch period, at 1:28 p.m. EST on Monday, November 18, 2013.

In addition, MAVEN carries an Electra communications relay package, designed to allow it to relay data between any of the landed assets and the Earth. At this writing, the *Opportunity* and *Curiosity* rovers are active on the surface, and development is proceeding for the *InSight* geophysics lander to be launched in 2016, the European Space Agency *ExoMars* lander and rover to be launched in 2016 and 2018, respectively, and the Mars 2020 rover to be launched in 2020. MAVEN will join *Mars Odyssey*, *Mars Reconnaissance Orbiter*, and *Mars Express* as having relay capability in orbit.

The MAVEN spacecraft was designed with a lifetime to ensure that it could survive its ten-month cruise to Mars, the five-week transition phase of commissioning the spacecraft, and its one-Earth-year primary science mission. Resources, including fuel, were conservatively allocated based on this lifetime. Anticipating that there will be fuel beyond that required for the primary mission, MAVEN can survive longer and continue its science observations and relay activities during an extended mission.

4.2 Science Instrument Accommodation

Each instrument has been accommodated in a way that best allows it to obtain its necessary science observations while minimizing impact or impingement from the spacecraft. The accommodation is described below for each instrument, and Fig. 9 shows the accommodation graphically.

There are three separate approaches for accommodating instruments. Three of the instruments (SWIA, SEP, EUV) required having a fixed orientation always pointing at the Sun or the direction of the solar wind. These instruments are body mounted on the spacecraft, in

available areas surrounding the HGA. As the planned operational modes most often point the spacecraft (and the solar arrays) at the Sun and have a fixed orientation relative to the solar wind, these instruments have their ideal orientations most of the time.

Three of the instruments (IUVS, STATIC, NGIMS) are located on an Articulated Payload Platform (APP) that is at the end of a 1.2-m deployable boom. There are two gimbals connecting the APP to the boom, giving two degrees of freedom in pointing the instruments. With the body of the spacecraft pointed toward the Sun, this approach allows these instruments to orient themselves independently from the Sun. That way, NGIMS can point its inlet into the ram direction during periapsis passes, STATIC can orient itself so that it can see the expected high-energy ions, and IUVS can see the side limbs during periapsis passes, the corona during the middle parts of the orbit, and the planet while near apoapsis.

The LPW probes are mounted on two 7-m stacer booms that are oriented at an angle relative to all three axes of the spacecraft. With this orientation, and with the probes extending past the edge of the solar panels, it is possible to ensure that both probes will not be in the sun shadow or spacecraft wake at the same time.

The SWEA instrument is on a separate 1.2-m boom extending up and back from the spacecraft body. The boom allows the instrument to be located at a distance from the spacecraft in order to minimize the effects of any spacecraft charging (see next section) on the measured electrons.

Finally, the two MAG sensors are located on small 0.68-m booms extending out from the distal end of the solar panels, getting them as far from spacecraft magnetic fields as possible. A rigorous magnetic cleanliness program (next section) ensured that the spacecraft and solar-panel magnetic fields are small enough that the necessary measurements can be made.

Each instrument has its required field of view, is located in a place that minimizes interference, and is away from thruster plumes.

4.3 Magnetic and Electrostatic Cleanliness

The requirements to measure weak magnetic fields and low-energy plasmas led to the adoption of four major cleanliness requirements. First, to measure the magnetic fields, the Orbiter may produce a static field magnitude of no more than 2 nT at the location of the magnetometers. Second, the time-variable magnetic field magnitude must be less than 0.25 nT, except for brief periods centered on transitions into and out of eclipse and instances of off-sun pointing. Third, to measure low-energy electrons and ions undisturbed by spacecraft-generated electric fields, the maximum tolerable variation in potential across any two points on the surface of the Orbiter must be less than 1 Volt. Finally, the ratio of grounded, conductive current collecting area on the Orbiter to the area of all surfaces at a biased potential must exceed 80.

Verification of the magnetic and electrostatic requirements was accomplished through the use of detailed mathematical models based on measurements of component properties. System-level measurements were used to verify the accuracy of the models.

Spacecraft Static Magnetic Field The Orbiter-level static field budget was managed without resorting to a policy of allocating limits to individual components. From experience (e.g., *Juno*, *MESSENGER*, *STEREO*) there are a limited number of components having significant impact to the static field budget. On MAVEN, these were propulsion components (latch valves and thrusters), reaction wheel assemblies (RWA), gimbal motors, traveling wave tube assemblies (TWTA) and the Electra UHF transceiver. The dipole moments of

all spacecraft components and instruments were measured prior to installation on the Orbiter. Most of the components were demagnetized, and structural elements were scanned for potentially magnetized areas.

The Orbiter construction with its open bay architecture, and with major subsystems colocated on panels, made it easy to reduce large component dipole moments. One major propulsion assembly contained all the latch valves, and the impact of these was reduced by the use of a small number of rare-earth magnets suitably placed and oriented so as to cancel out the component magnetic fields. Prior to the installation on the Orbiter, the effect of this compensation was verified at the panel level using a geometrically accurate fixture. Similarly, all the major X-band communications components (TWTAs, waveguide switches and transponders) are mounted on a single panel. These also were compensated at the assembly level. The Electra UHF transceiver was the only individual component on the Orbiter with its own compensation magnet. No Orbiter-level compensation was required. The bulk of the component magnetic-characterization measurements were performed at the Lockheed-Martin facility with the remainder either at Berkeley SSL or Ball Aerospace in Boulder, CO.

Numerous small items were screened and demagnetized as necessary. These included stainless steel fasteners, pyro valves and separation nuts. A rigorous magnetics control process was instituted during spacecraft assembly, with a control area around the Orbiter requiring special training and tool processing. A magnetically sensitive area around each magnetometer required the close involvement with the magnetometer team for all processing.

The Orbiter static moment model was verified by using a "swing" test where the Orbiter was suspended from an overhead crane and allowed to swing in pendulum fashion after a 75 cm displacement from the vertical. This was done for two axes. Then the Orbiter was rotated about the vertical (Z-axis) in the clockwise and counter clockwise directions. Data was taken with three nearby magnetometers. The pendulum motion modulates the signature and allows the extraction of the field due to the Orbiter. For this test, the major differences from a flight configuration were that the APP was stowed, and several components that were magnetically insignificant had not yet been installed. There was good correlation between the measured and predicted results.

Spacecraft Variable Magnetic Field Varying currents and moving permanent magnets produce the variable magnetic fields. Enforcing twisted wire pairs, adjacency of power and return lines, a prohibition on chassis returns, and single-point grounding of electronics minimized current-driven dipole moments in the harness. Close attention was paid to power and ground pin locations in connectors to minimize dipole areas. There were no requirements placed on electronics board layouts given the relatively low current levels and the approximately six-meter distance to the magnetometers. No compensation loops were implemented; however, all heater circuits were counter wired.

The magnetometer placement 0.68 m away from the distal edge of the solar array followed the approach used on the *Mars Global Surveyor* mission (Acuna et al. 2001). This effectively gave each magnetometer its own six-meter boom, leaving the issue of mitigating the solar-array current-driven fields. MAVEN did not perform aerobraking at Mars, allowing the backside of the solar array panel to be used for compensation wiring. A self-compensation scheme was used (see Fig. 10) where the solar cell string is formed into an effective current loop with a counter loop directly underneath on the backside of the panel. This was replicated over the panel with alternating polarities. The effect is to leave a cancellation "notch" around each magnetometer where the field is about 0.045 nT. Special care was also taken to ensure that effects from switching sets of strings were minimized.

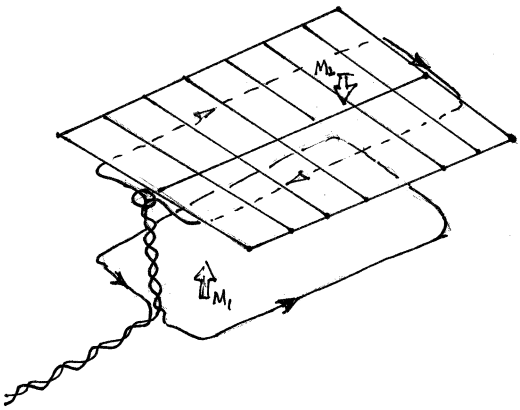

Fig. 10 U-string geometry for minimizing induced magnetic fields in the solar arrays. Return wires on the back side of the solar arrays go in the opposite direction from the current generated on the front side by the solar cells

The two lithium-ion batteries were wired with a serpentine harness and optimized cell orientation. They were then shielded with a 20-micron high-permeability foil. Fields from the batteries are on the order of 0.020 nT at peak discharge currents.

The rotating components (RWA, APP gimbal motors) and the ACS thrusters were all wrapped in the 20-micron high-permeability foil. This reduced their variable fields to levels well within the requirements. While an ACS thruster cannot be completely shielded, the worst-case combinations of all thrusters firing was examined and the effects were found to be small. The motors for the scan and grating flip mirrors of IUVS were magnetically measured early in the program; their impact was small, not needing special treatment. The EUV aperture window was also measured in open and closed positions, and it too did not need special treatment.

The effect of the APP motion was the most complex to model as it involved reorienting rotating machinery that is also varying in distance to the magnetometers. While the rapid field variation from the motor elements is relatively small (~ 0.020 nT), the slew motions of the APP will produce infrequent (2 to 10 times per orbit) magnitude variations on the order of 0.140 nT.

An extensive powered magnetics survey was conducted as part of the environmental test program. The objective was to verify the current-driven models and discover any inadvertent current loops while there was time to fix them. Four 3-axis magnetometers were used at three locations approximately 0.5 m distant around the spacecraft on the assembly floor. All electronic components and heater circuits were cycled individually and their signatures recorded. The non-flight aspects of the powered configuration were accounted for, as well as the fact that these measurements were conducted in Earth's ambient field and in a magnetically noisy environment. Current-structure size was accounted for when computing the expected fields as the dipole approximation is not always valid. In addition to the powered testing, an APP motion test was conducted, and consisted of several cycles of APP motion in both the outer and inner gimbal angles. This test verified the APP moments and field structure. These tests and extensive modeling showed the expected static and variable fields to be within the required limits.

Calibration maneuvers in which the spacecraft is rolled about its principal axes have been carried out both during cruise and during orbital operations. These will allow us to confirm the magnetic properties in flight and to measure any time variability.

Electrostatic Cleanliness We wished to minimize differential charging on the spacecraft that would affect measurements of the electron or low-energy ion populations. This put a

premium on ensuring that the surfaces were sufficiently conductive through electrical design requirements and materials selection.

The bulk of the exposed Orbiter surface consists of solar cell cover glass, a moderately conductive solar array panel, multi-layer insulation (MLI) blankets, and metal structure. With the first two items being dictated by program decision, the focus was then on ensuring the adequate conductivity of the MLI blankets and their grounding. MAVEN uses the same blanket technology as the *Juno* spacecraft and exhibits conductivity more than adequate to meet the MAVEN 1-V variation requirement. This requirement is based on a nominal 4 nA/cm^2 current density. The use of large electrically conducting blankets to close out the equipment bays resulted in the spacecraft body structure appearing largely as a grounded box to the surrounding plasma. Close attention was paid to the grounding of components and blankets. This simplified the problem by establishing separate, connected equipotential planes for the APP and the spacecraft body.

Analysis of the field behavior was performed using a combination of analytical models and NASCAP, an industry standard software tool for spacecraft electrostatic analysis (Mandell et al. 2006). These showed that differential charging of the spacecraft would have a small impact to the observations of charged species made by SWEA, STATIC and NGIMS, although the cell-side of the solar array does not comply with the electrical conductivity requirement.

Spacecraft Current Balance Missions with Langmuir probes ideally are expected to have a minimum ratio of grounded surface to biased metal surface of several hundred (Brace 1998). This ratio is based on the expected ion and electron currents in the ionosphere, and keeps the probe operation from perturbing the spacecraft potential with respect to the plasma.

MAVEN has minimum ratio of 80. This occurs when the spacecraft is in sun-velocity mode (see Sect. 5) and the ram vector is in the +Z half-plane. The ratio is on the order of 200 to 400 in other operation modes, and also when the ram vector is in the −Z half-plane. Detailed calculations for a range of plasma and illumination conditions were performed using conservative estimates of the Orbiter photoemission characteristics. These calculations show that the variation of the spacecraft potential is negligible for the expected plasma environments during Langmuir probe operation.

EMI Impact to Instruments The electrical design rules described above also helped suppress emissions into sensitive payload receiver bands. Orbiter-level testing showed that the spacecraft would meet the requirements of the LPW instrument in its waves mode. Additionally, the Electra payload with its sensitive UHF receiver was shown to perform satisfactorily while the spacecraft was operating.

4.4 Radiation and Radiation Background Controls

Observation of the response of the upper atmosphere system to Solar Energetic Particle (SEP) events, such as solar flares, is one of the primary observational goals of the MAVEN mission. We have little insight into the relationship between SEP input and atmospheric response, either at Mars or at Earth. Determining this relationship requires making SEP and upper-atmospheric observations at high time resolution and by observing the event to the fullest degree possible.

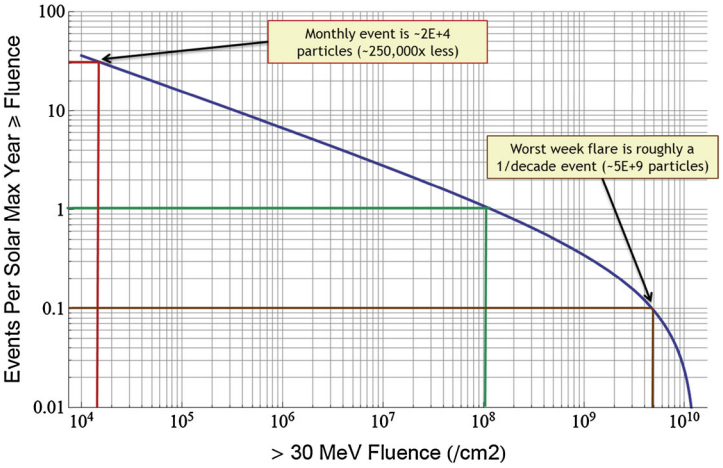

Fig. 11 Expected fluence frequency distribution of energetic particles at the MAVEN spacecraft. The largest expected event is indicated by the *brown line* and is equivalent to the "Halloween" storm in 2003

Solar flares are dynamic events spanning several days. Given the variability within and between events, observing the full sequence of both solar input and atmospheric response by having consecutive orbits of data is necessary to understand the event. Observations of multiple events are required in order to understand their impact on the system because of both their different energies and differences between events.

Therefore, the MAVEN spacecraft and instruments need to be capable of continuous observation through such an event. Such events are also a source of Single Event Upsets (SEUs) in electronics. Should an SEU occur in a critical spacecraft component, the spacecraft could enter safe mode have a reboot of the space flight computer. In either case, science operations would be suspended for several days. A reboot is more significant because it could result in a loss of the science data collected in the days leading up to the upset.

Early in the design effort, we conducted an SEU susceptibility analysis to determine the probability of the spacecraft experiencing an SEU that would interrupt science operations during an SEP event. This required a part-by-part review of the spacecraft's electrical components to identify parts that were susceptible to upsets and had the potential to interrupt science operations. Engineers estimated the probability of upset for each susceptible part when exposed to an extreme solar flare event, using the "Halloween Storm" of October 2003 as our worst-case example (Baker et al. 2004; Crider et al. 2005). This is roughly a once per decade event, shown on the brown line in Fig. 11. The concept of a "worst week flare" is meant to describe the likelihood that this worst flare would occur in a given week, not just on a given day or at some time during the mission.

The individual part probabilities were then combined to determine that the MAVEN spacecraft has an overall probability of approximately 85 % of continuing science operations through this worst-case flare event. As seen in Fig. 11, the relative intensity of more-common flares is significantly less than the Halloween storm. The extreme storm contains approximately 250,000 times more highly energetic particles than storms that are expected on a monthly basis. Since upset probability decreases with the number of highly particles, it is expected that MAVEN will provide higher reliability throughout the duration of the mission.

4.5 Planetary Protection

As with all planetary missions, MAVEN is required to meet the appropriate planetary protection requirements. For a Mars orbiter, the objective is to ensure that we minimize contamination of Mars that can affect future scientific investigations. We have taken the following steps:

Centaur Upper Stage The MAVEN spacecraft was injected into its heliocentric transfer orbit to Mars by the Centaur upper stage. The upper stage and spacecraft were targeted in a way that off-points them from Mars to ensure that the probability that the upper stage will hit Mars within 50 years is less than 10^{-6}. The first trajectory correction maneuver (TCM), carried out approximately two weeks after launch, removed most of this offpoint and was used to put the spacecraft onto the proper trajectory to get to Mars. The upper stage does not participate in this TCM, and continues on its off-pointed trajectory. In addition, after separation from the spacecraft, remaining fuel is used to push the upper-stage trajectory even farther away from Mars.

Spore Delivery Consistent with the Committee on Space Research (COSPAR) planetary protection panel international agreements, MAVEN has taken steps to ensure that it delivers fewer than 500,000 spores to the surface of Mars at any point in its lifetime. The spore burden delivered to the surface is reduced to this number by several means:

(i) Assembly and test in a class 10,000–100,000 clean room, using protocols that minimize the contamination.
(ii) Microbial assays of numerous components at multiple stages to ensure that contamination has been minimized and to aid in tallying up the number of spores on the components.
(iii) Analysis of the component heating that will occur during the eventual entry into the Mars atmosphere, to determine the degree of sterilization of components. This calculation, called "breakup and burnup analysis", tracks the spacecraft heating on entry, the breakup of the spacecraft due to either aerodynamic forces or heat-induced deterioration of attachment points, the trajectory and heating of individual components, and the effects on component and total spore burden.

Reviews of our planning and implementation process are carried out by the NASA Planetary Protection Officer to ensure compliance. The end result of the analyses suggests that, when MAVEN eventually impacts Mars well after completion of its science mission, it will deliver between 50–70 % of the allowable spore burden to the Martian surface.

5 Mission Plan

5.1 Mission Phases

The MAVEN mission can be divided up into discrete phases for ease of both planning and discussion. They are the pre-launch phase, launch phase, cruise, Mars orbit insertion (MOI), transition phase, primary science, extended science and relay. Each is briefly discussed below. Figure 12 shows a timeline showing all of the phases.

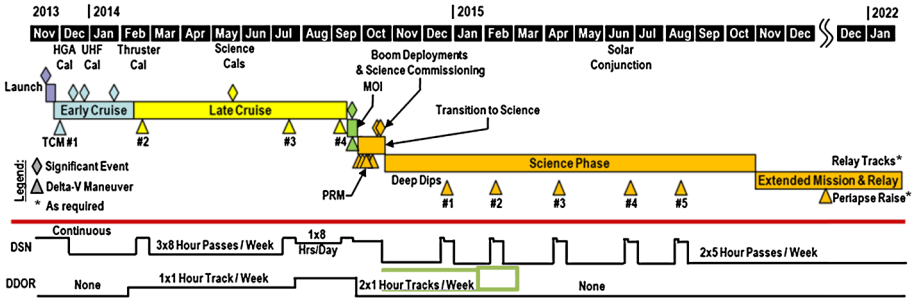

Fig. 12 Overall timeline of MAVEN mission, from launch through end of primary science mission and into a possible extended mission

Pre-launch Pre-launch phase ran from when the spacecraft was shipped to Kennedy Space Center and Cape Canaveral Air Force Station for preparation for launch until we entered the launch phase about four days prior to launch.

Launch MAVEN could launch during a 20-day launch period, from 18 November–7 December 2013. The limits on this are set by the launch vehicle capability given our final spacecraft mass and by the ability of the onboard fuel to allow us to enter Mars orbit. As our final mass was under the "not to exceed" launch mass, the viable days for the launch period extended somewhat, and we could launch for up to two weeks past this nominal date and still have fuel to carry out our primary mission.

Launch phase began at final power-up of the spacecraft for launch at L-102 hours and continued after launch until the spacecraft team determined that it was safe to transition to cruise mode. Transition to cruise was expected to occur at about L+1 day. Prior to lift-off, the spacecraft switched from external to internal power at L-9 minutes. Lift-off was sensed by the launch vehicle with mechanical break-wires, and triggered the script that ran during the boost phase and prepared the spacecraft to operate once separation from the upper stage occurred.

Separation occurred about 47 minutes after lift-off, and triggered automatic entry into safe mode. Safe mode automatically configured the spacecraft, damped any rotation rates left from separation, triggered deployment of the solar arrays, determined orientation of the spacecraft, and slewed the spacecraft to a predetermined safe attitude. At that point, high-data-rate flow of telemetry began, and the team was able to assess the condition of the spacecraft. Once the spacecraft was in a safe, known state, it was able to transition to cruise mode.

Cruise The spacecraft took ten months to get to Mars on a heliocentric orbit. The spacecraft was on a Type II trajectory, taking just over one half of an orbit around the Sun to reach Mars. During this time, spacecraft and instrument calibration and testing occurred, and TCMs were carried out to ensure an appropriate trajectory and approach to Mars.

Four TCMs were scheduled during the cruise phase (with additional opportunities during the MOI phase). The first was carried out using the MOI thrusters as a dress rehearsal for the processes and procedures to be used for MOI.

The Cruise timeline is shown in Fig. 13. Each instrument carried out aliveness tests, functional tests, and performance tests, and several of the instruments carried out calibrations by observing the Sun, stars, or the solar wind. Spacecraft calibrations included solar, thruster,

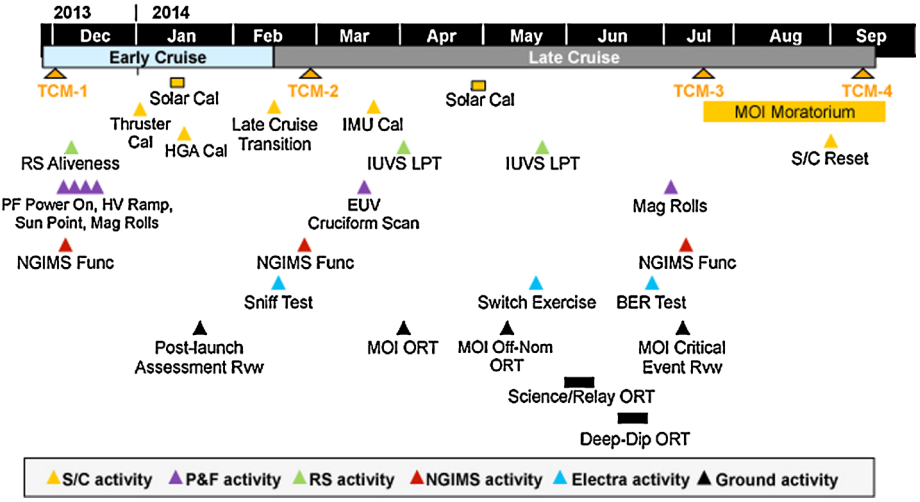

Fig. 13 Cruise Phase timeline of planned events, showing when they were *scheduled*

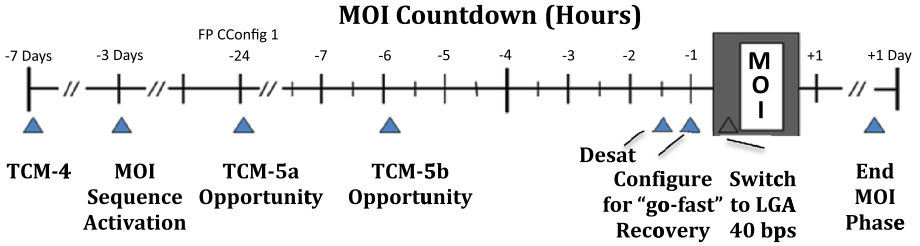

Fig. 14 Sequence of events during the MOI phase. MOI phase ran from MOI – 3 days until declaration at about +1 day that we had switched to transition phase

and IMU calibrations. A command moratorium was in effect for 60 days prior to MOI to ensure that the team was able to focus on the upcoming major MOI event.

MOI The MOI phase began at MOI-3 days when the MOI sequence was activated. At that point, no further intervention from the ground was required in order for the spacecraft to execute its MOI burn. There were two opportunities planned for last-minute emergency TCMs, at MOI-24 hours and MOI-6 hours, in case there were serious problems with the approach trajectory (see Fig. 14).

The MOI burn was approximately 33 minutes duration, and successfully placed MAVEN into its desired 35-hour orbit. The spacecraft fault protection during MOI had autonomous recovery from a safe-mode entry during this phase and a "go fast" recovery mode that included use of thrusters to reacquire proper attitude. If a fault occurred during the MOI burn, the spacecraft could autonomously recover and resume the burn. The worst case of swapping C&DH sides, reacquiring attitude, and resuming the burn would have required 13 minutes; in such a case, the spacecraft would still enter a safe orbit, and it carried sufficient fuel to get from this longer-period orbit to the science mapping orbit if necessary. Communications during the burn was not possible on the high-gain antenna because the spacecraft was aligned for the burn and the antenna did not point at the Earth. There was communications

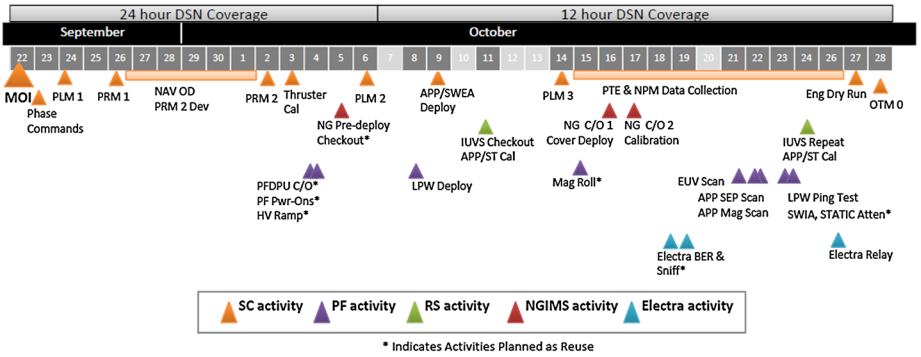

Fig. 15 Nominal timeline of activities for the Transition Phase. Activities occur on almost every day, with days of no activity being shown in *light gray*. As actually implemented, five days were inserted for observations of Comet Siding Spring which had its close approach to Mars on Oct. 19

through the low-gain antenna, but the low bit rate precluded any significant downlink of data; however, use of the LGA allowed tracking of the spacecraft and the velocity change through the burn using the Deep-Space Network antennae here on Earth. After safe orbit insertion, transition to the Transition Phase occurred; from the spacecraft perspective, the difference between MOI Phase and Transition Phase was mainly in the area of any fault-protection responses to problems.

Transition Phase We had scheduled a five-week transition phase in order to execute propulsive maneuvers to get into the science mapping orbit, to do a post-MOI thruster calibration, to deploy the science booms, to test and check out the science instruments, and to do key calibrations. Figure 15 shows an overview of the Transition Phase timeline. The dates shown assume a launch on the first day of the launch period; a delay in arrival due to a delay in launch would have pushed back the date of MOI and the start of the transition phase.

Five maneuvers were used to lower periapsis and to reduce the period (lower apoapsis) to get to the final science orbit. Discrete maneuvers occur either at apoapsis (for the Periapsis Lowering Maneuver, PLM) or at periapsis (for the Period Reduction Maneuver, PRM, which lowers apoapsis).

After completion of the transition phase, we began our science mapping. We had not defined formal criteria that allowed us to declare the end of transition; there were too many possible scenarios involving possible problems with instruments or calibrations to work through. If issues arose, we had the ability to delay the start of mapping or to begin mapping without having all of the instruments fully operational.

Primary Science The primary science mission lasts for one Earth year. This period was selected in order to allow the expected variation of the solar inputs during the declining phases of the solar cycle to provide significant variability in the input conditions. By measuring the response of the system under varied boundary conditions, we can obtain information that lets us extrapolate back in time and determine the integrated loss to space through time. The MAVEN orbit is elliptical in order to allow *in situ* sampling of the entire column of the upper atmosphere and to allow quasi-global imaging from high altitude at apoapsis. The orbit has a nominal periapsis altitude of 150 km, apoapsis altitude of 6220 km, and period of 4.5 hours (Fig. 16)

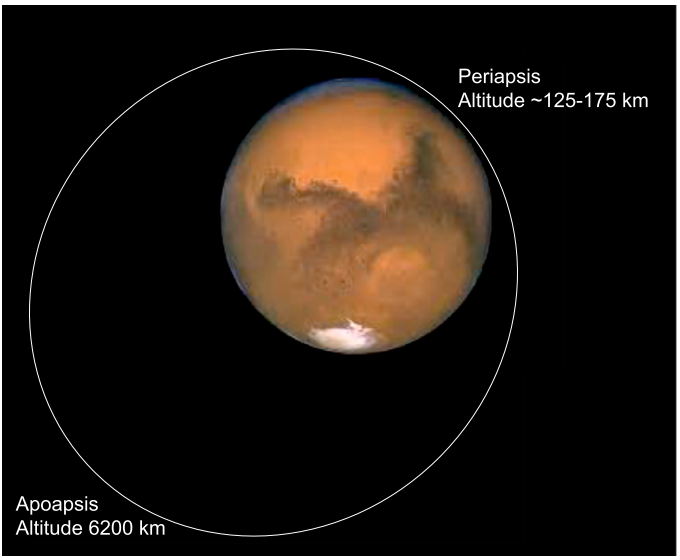

Fig. 16 Nominal MAVEN orbit shown to scale with Mars

The periapsis is targeted toward an atmospheric density rather than an altitude, with the density range within this corridor being between 0.05–0.15 kg/km^3. Actual altitude varies depending on season, location, and surface elevation. Periodic Orbital Trim Maneuvers (OTMs) are carried out in order to keep the periapsis within this density corridor.

The apoapsis altitude, orbital period, and orbital inclination (75°) were chosen to provide appropriate rates of precession of the orbit in both local time and latitude of periapsis as driven by the non-symmetric gravitational field. With the orbit precessing, observations can be made at all local solar times and at all latitudes between $+/-75°$. Figure 17 shows the trace of periapsis latitude and local solar time throughout the mission.

Each orbit is divided up into four orbital segments, with different observations or modes planned for each segment. Figure 18 shows this graphically. The four segments consist of:

- Periapsis segment. Observations emphasize composition and structure from the nominal periapsis altitude of 150 km up to an altitude of 500 km.
- Inbound/outbound segments. Observations emphasize measurements of the hot corona and of escaping species at intermediate altitudes.
- Apoapsis segments. Observations emphasize quasi-global IUVS observations of the planet's disk.

During science operations, there are a limited number of modes in which the spacecraft can operate. Each mode consists of a particular orientation of the spacecraft and of the APP during each of the legs in the orbit. While one can imagine wanting infinite flexibility in combining different observations on the different legs, there actually are a limited number of useful combinations; we simplified the planning and implementation of the sequences by using the minimum number of possible combinations. Table 6 lists the observations that can be made during each orbital segment, and which can be combined into ten different science scenarios. Each is characterized by a sequence of two orbits, with each of the eight segments over the two orbits having a specified observational mode.

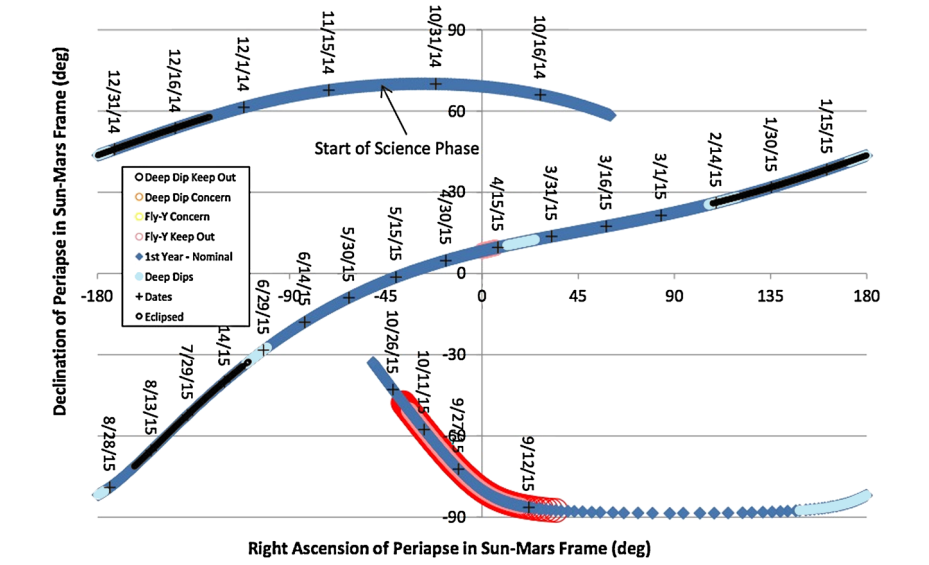

(a)

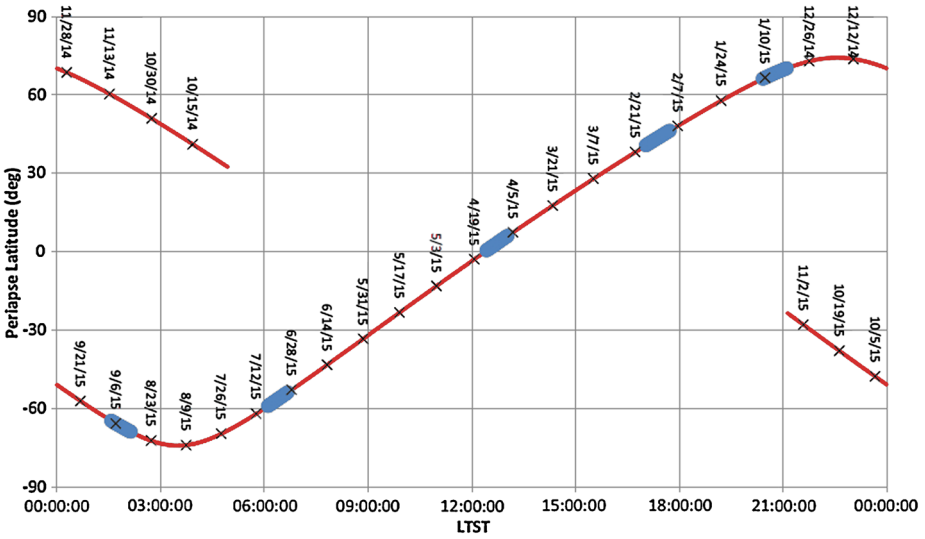

(b)

Fig. 17 Trace of the MAVEN orbit through the primary science mission. (**a**) Periapsis location in "MSO" coordinates, relative to the subsolar latitude and longitude. (**b**) Periapsis location in "geographic coordinates", showing the latitude and local solar time of the sub-spacecraft point. (**c**) Periapsis location shown as a function of the latitude of the ascending node of the orbit and local solar time. In each panel, calendar dates of the planned deep-dip campaigns and actual dates through the mission are shown. The first panel also shows some of the constraints that affect planning of the deep dips

The preference is to use scenario 1 whenever possible. With this scenario, the spacecraft alternates between being solar-pointed during periapsis and being aligned along the ram direction during periapsis However, spacecraft, instrument, or observational constraints make

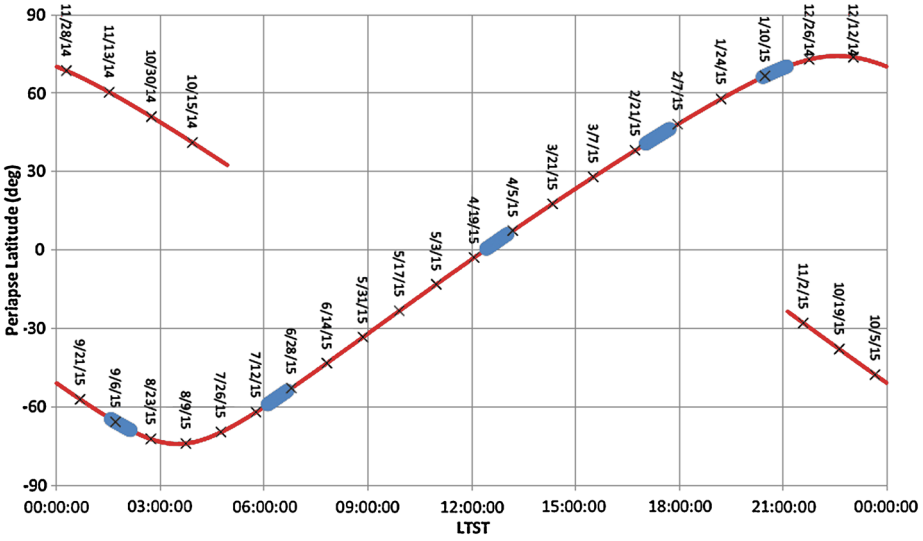

(c)

Fig. 17 (*Continued*)

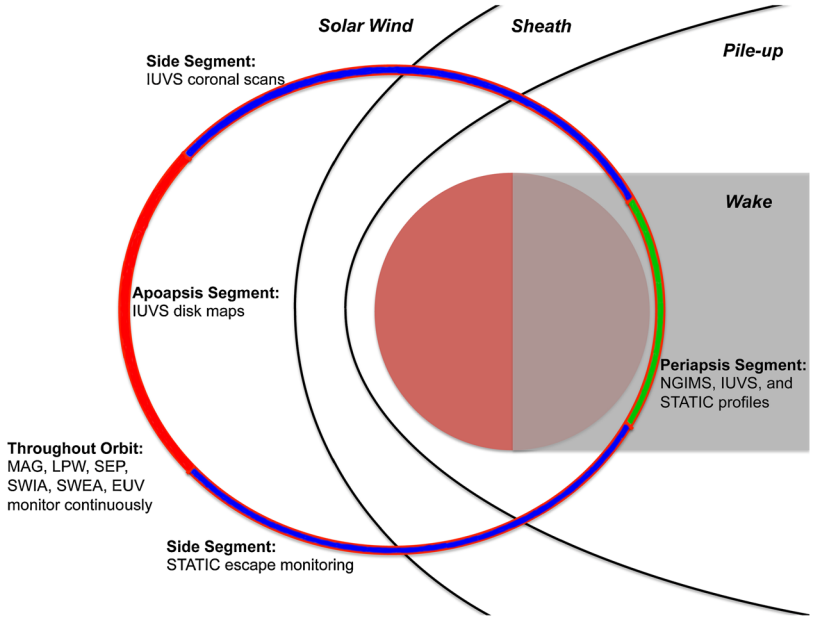

Fig. 18 Types of observations made during each of the four segments into which the orbit is divided. Orientation with respect to the magnetosphere is representative, as the orbit precesses in both periapsis latitude and local solar time. Sun is to the *left*

Table 6 Observational modes. MAVEN uses ten different observational scenarios, each having a different combination of observations using the following components

Orbit segment	Purpose	Description
Apoapse segment	IUVS disc scan	IUVS points at planet with fixed orientation, spacecraft motion allows imaging of visible disk
Side segments	IUVS coronal scan	IUVS observes across orbit, spacecraft motion provides vertical scan through hot H and O corona
	STATIC sun-nadir	STATIC field of view is oriented to contain sun and nadir vectors, with spacecraft motion providing vertical scan through coronae
Periapsis segment	Fly-Y	Spacecraft Y axis oriented along velocity vector; allows IUVS limb scanning
	Sun-velocity	Spacecraft Z axis pointed toward sun
	Fly-Z	Spacecraft Z axis pointed along velocity vector; used for deep-dip campaign
Earth point	Comm. with Earth	Spacecraft Z axis and HGA align with Earth

it impossible to use this mode at certain times; other modes are substituted. The nominal timeline (Fig. 19) shows the planned modes throughout the primary mission.

Five times during the primary mission, we will lower periapsis to an altitude of approximately 125 km (actually targeting a density corridor of 1.5–3.0 kg/km^3). At this altitude we are in the vicinity of the homopause that separates the diffusion-stratified upper atmosphere from the well-mixed lower atmosphere. Carrying out these "deep dip" observations allows us to profile the entire upper atmosphere down to where it connects to the lower atmosphere. We do this only at selected times in order to minimize drag on the spacecraft that would alter its orbit (as in aerobraking) and to minimize the risk of high-voltage arcing that could damage some of the instruments. Those instruments at risk from high-voltage arcing are turned off for the periapsis passes during the deep dips.

The deep dip is carried out for approximately 20 consecutive orbits over five days. These orbits all occur at essentially the same periapsis latitude. Planetary rotation allows us to observe at periapsis at 20 different longitudes. The preliminary times selected for the deep dips allow us to observe at high latitudes, the dawn and dusk terminators, near the subsolar point, and on the nightside.

Final decisions on timing and placement of the deep dips will be made after science measurements begin and we can see how the processes in the upper atmosphere are operating. The major operational constraint on carrying out the deep dips occurs when the spacecraft passes through the Mars shadow near apoapsis. Although the batteries were sized so that these eclipses would not be an issue, the combination of having a lengthy eclipse plus pointing off Sun for the deep-dip pass could drain the batteries too much; exclusion periods have been identified during which a deep-dip campaign may not be carried out.

Relay Capability The MAVEN spacecraft carries with it an Electra UHF relay communications package that allows it to act as a data relay for surface assets. This type of relay has been the primary means of returning data to Earth from the *Spirit*, *Opportunity*, and *Curiosity* rovers, with the *Mars Odyssey* and *Mars Reconnaissance Orbiter* providing that relay link. In addition, it is being planned as the primary data link for the *ExoMars* Entry Demonstrator Module (EDM) and the *InSight* geophysical lander, both to be launched in 2016. MAVEN is the backup relay to both *ODY* and *MRO*, but is expected to be utilized

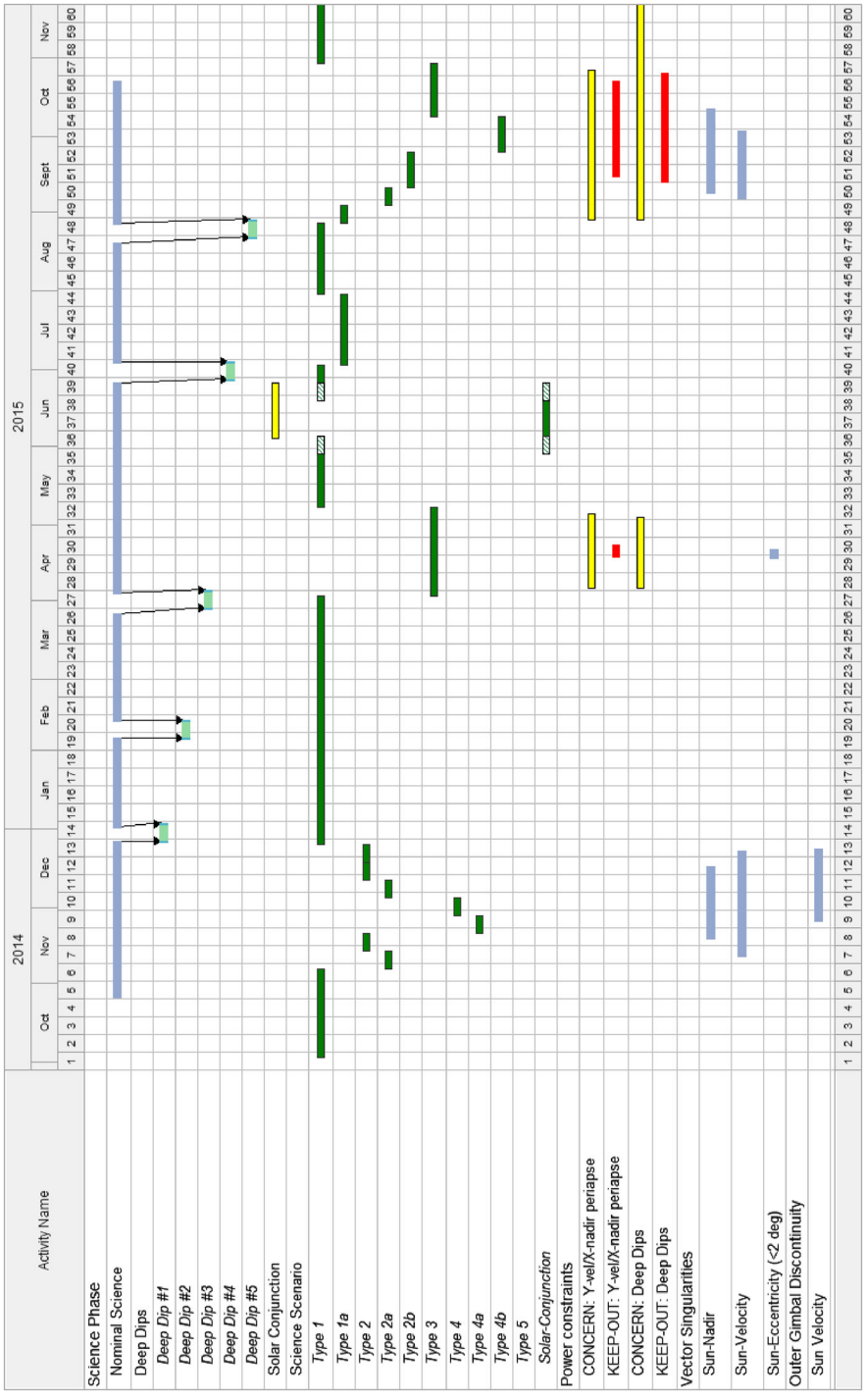

Fig. 19 Planned modes throughout the science mission. Science scenarios indicated correspond to those identified in Table 8. Constraints are shown that preclude using certain scenarios at certain times. Week of the science mission is identified in the *third line* across the top

following MAVEN's primary mission. MAVEN generally cannot carry out both relay communications and its own science observations on the same orbit, but we anticipate that it can carry out both effectively over the course of the multiple orbits on a single day if necessary.

Extended Science and Relay After the one-year primary mission, we anticipate having sufficient fuel to support continued science and relay operations. The actual fuel usage for nominal operations will not be known until we have significant experience in orbit. As we did not have to recover from an MOI reset and can use the fuel allocated for such a recovery for operations, and using our nominal estimates for fuel consumption during science operations, then we should have sufficient fuel for: One Earth year of science operations during the primary mission, five deep-dip campaigns during the primary mission, approximately 28 months of continued science operations from our nominal orbit (no deep dips), then raise periapsis and have an additional six years of long-duration extended-mission science and relay operations. Of course, fuel can be allocated differently, choosing to have a shorter extended mission in order to carry out deep-dip campaigns during the extended mission, or choosing to have a shorter extended mission in order to have a longer long-duration extended mission. There are both scientific and programmatic aspects of those trade-offs, and no decisions on detailed implementation have been made.

Spacecraft Disposition MAVEN's planetary protection implementation does not require us to carry out a maneuver to raise periapsis in order to get to a long-lived "planetary quarantine" orbit. The ultimate disposition of the spacecraft will be decay of the orbit, entry into the atmosphere, and impact onto the surface. Once we raise periapsis to get into our long-duration extended-mission orbit, impact would not be expected to occur until decades following the end of the mission.

6 Science Closure and Anticipated Results

6.1 MAVEN Science Closure: from Measurements to Answers

After obtaining the MAVEN measurements, we require a coherent and comprehensive strategy for turning instrument data into responses to our top-level science goals. The MAVEN strategy for characterizing the upper atmospheric reservoir (goal 1) and determining atmospheric escape rates today (goal 2) and through time (goal 3) are described in detail in companion papers by Bougher et al. (2014) and Lillis et al. (2014) respectively. Below we briefly summarize the global models that will inform physical interpretation of MAVEN data, as well as our science closure strategy.

6.2 Goal 1: Determine the Composition, Structure and Dynamics of the Upper Atmosphere and the Processes Controlling Them

MAVEN's suite of instrumentation will allow us to characterize the current state of the Mars upper atmosphere, in particular its composition, structure, dynamics and the physical processes that drive its variability. We adopt a broad definition for the Mars upper atmosphere, taking it to extend from the top of the well-mixed lower atmosphere all the way out to the tenuous exosphere. We take it to include neutrals, electrons, ions, photons and electric and magnetic fields—the entirety of the neutral and ionized portions of the atmosphere and their interaction with the solar wind.

This characterization will be achieved via individual case studies, statistical investigations, the construction of empirical models of upper-atmospheric structure, and comparison with a variety of relevant physical models of the Martian upper atmospheric system and solar wind interaction. We categorize the regions of study as comprising the thermosphere, ionosphere, exosphere and magnetosphere.

Thermosphere Measurements from ACC, NGIMS and IUVS will allow, for the first time, a comprehensive characterization of the basic structure of the Martian thermosphere and its geophysical variability. We will build up a three-dimensional picture of the composition, temperature and density of the thermosphere above ~ 100 km in addition to the location of the important homopause and exobase boundaries and how all of these vary with season, solar activity and solar zenith angle. This will enable us to investigate topics concerning the thermosphere such as winter polar warming and its hemispheric asymmetry, thermal tides, gravity wave propagation from the troposphere, joule heating from particle precipitation, dust-storm effects and a better understanding of CO_2 radiative cooling. Also we will have some capability via NGIMS and ACC to investigate zonal and meridional winds and how they vary.

Ionosphere Measurements of ion densities from NGIMS and IUVS, ion temperatures from STATIC, and electron densities and temperatures from LPW will allow, also for the first time, a reliable characterization of the structure of the Martian ionosphere. We will understand better the formation of the different ionospheric layers (see review by Withers 2009) and their drivers. Knowledge of ionospheric photochemistry will be improved by ion composition measurements on every orbit (versus having only the two dayside vertical profiles measured by the *Viking* Landers during entry in 1976) as well as the first ever measurements of plasma temperature below 220 km. Additionally, the poorly understood patchy and irregular nightside ionosphere will be comprehensively sampled. This will enable us to investigate relevant ionospheric topics such as wind-driven currents, ring-current-like crustal field curvature and gradient drifts, electro-jets, cross-terminator ion flows, electron-impact ionization, auroral effects, SEP ionization and airglow.

Exosphere Though NGIMS will measure neutral densities down to 10^3 cm^{-3}, IUVS coronal scans will be the primary tool for investigating the Martian exosphere. Robust retrieval algorithms will enable characterization of the basic structure and variability of the oxygen and hydrogen exospheres of Mars by providing density and temperature as a function of altitude and solar zenith angle. This will enable the investigation of some basic exospheric science topics such as day-night asymmetries and how they vary with season and EUV flux, the relative contributions of bound and unbound particles to the exosphere, the relative contributions to the exosphere from sputtering and photochemical energization processes, and the influence of the lower atmosphere (e.g., water vapor connections to Hydrogen Lyman-alpha enhancements).

Magnetosphere A comprehensive suite of space plasma instrumentation (SWEA, SWIA, SEP, LPW and STATIC) will enable a full characterization of the current state and variability of the induced magnetosphere. The MAVEN orbit will take it into the undisturbed solar wind during portions of the orbit for as much as 80 % of the nominal mission, allowing a statistical picture to be built up of magnetospheric structure, in particular the locations and variability with solar drivers of the important plasma boundaries: the ever-present bow shock and magnetic pileup boundary (MPB) and the more-transient ionopause and photoelectron boundaries. In addition to global structure, MAVEN will enable investigation of

numerous topics in the Martian magnetospheric dynamics—plasma waves upstream of the bow shock, magnetosheath turbulence, draping asymmetries at the MPB related to the IMF, plasma instabilities at the MPB, flux ropes and their relationship to crustal fields, magnetic reconnection/plasma acceleration, plasma sheet/magnetotail dynamics, returning planetary ions from the deep tail, the properties, locations and frequency of current sheets, and the effects of coronal mass ejections and other solar wind disturbances on the magnetosphere.

6.3 Goal 2: Determine the Escape Rates at the Present Epoch and How They Relate to the Controlling Processes

MAVEN's second top-level goal boils down to answering the following question: How and why do the escape processes depend globally and locally on external factors such as solar EUV flux and solar wind pressure, and on planetary coordinates/variables such as solar zenith angle, dust activity and the topology and strength of the crustal field?

Despite the tightly focused suite of integrated investigations onboard the MAVEN spacecraft, *in situ* coverage is limited to points along MAVEN's orbit, while IUVS data will return a shorter list of derived quantities (see McClintock et al. 2014). Also, escape is measured directly only for ions (by the STATIC instrument); neutral escape rates must be inferred through coronal scale heights and by measurements of processes such as pick-up-ion sputtering that can produce energetic atoms. Lastly, whether MAVEN makes escape measurements over a representative range of solar conditions thought to have been prevalent over solar system history depends on the behavior of the Sun during the primary mission. In order to bridge these measurement "gaps" (spatial, temporal, and with respect to solar inputs and upper atmospheric processes and quantities), it is necessary to closely integrate several types of physics-based models with multi-instrument analysis of MAVEN data. Here, we discuss MAVEN strategy for constraining each of the six likely loss processes.

Jeans Escape Jeans escape only occurs in non-negligible quantities for hydrogen, deuterium, and helium at Mars. It will be constrained locally by NGIMS and IUVS measurements of densities and temperatures (from scale heights) of H and H_2; use of a Boltzmann calculation will provide the fractions of the distribution with escaping velocities and hence the thermal escape fluxes. For the IUVS coronal scans of the hydrogen exosphere, the escape rates will be derived by modeling the escape rates using the measured exobase densities and coronal density profiles.

Photochemical Escape Although photochemical escape will not be observed directly by MAVEN, all the relevant quantities upon which it depends will be measured. LPW will measure electron density and temperature, NGIMS and IUVS will measure neutral and ion densities, and STATIC will measure ion velocities. Every periapsis pass will produce an inbound and outbound altitude profile of these quantities that can be compared with models. First, a photochemical model (Fox and Hać 2009) will take these profiles (primarily ions and electrons) as input and calculate the energy distribution of hot O, C and N atoms at each altitude. Next, a Monte Carlo model of hot-atom transport will ingest these profiles and neutral densities and will calculate escape fluxes at the latitude and longitude (solar or geographic) of exobase crossing. In this way, a global picture of photochemical escape will be built up for different combinations of external conditions (e.g., a small range of EUV flux). 3-D global models of hot-atom escape (see Lillis et al. 2014) will be used to interpolate across global escape maps to calculate global photochemical escape rates and how they vary with the controlling drivers.

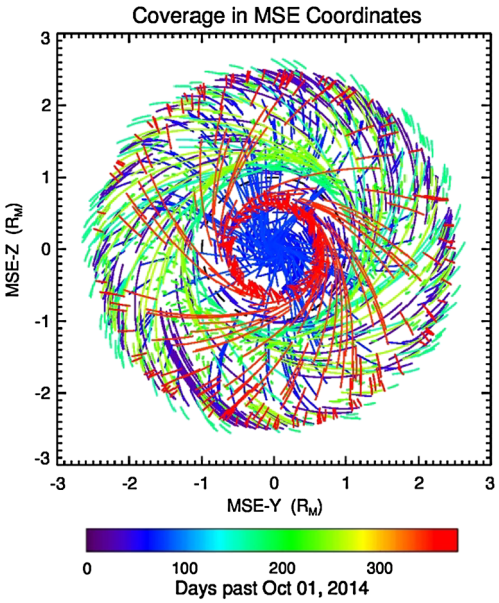

Fig. 20 MAVEN's coverage at a distance of 0.4 Mars radii downstream from Mars, *colored* according to time as indicated. Coverage is shown in MSE coordinates, assuming each orbit segment occurred during a steady IMF clock angle direction drawn from the distribution of clock angle directions recorded during the Mars Global Surveyor mission and presented in Brain et al. (2003)

Sputtering Escape As MAVEN will not directly measure escaping neutrals and their energies, we plan to derive sputtering escape rates using two complementary indirect techniques. The first technique uses *in situ* measurements from STATIC of downward-traveling pickup ions to build up "precipitation maps" of sputtering agents (mostly oxygen ions), with gaps in coverage being filled by global models of precipitating ion flux (e.g., Fang et al. 2008; Curry et al. 2013). These maps will be combined with atmospheric neutral density profiles from NGIMS as inputs to models that calculate the sputtered escape rates of O atoms. The second technique uses IUVS measurements of the hot oxygen corona and attempts to first isolate the sputtered component from the photochemical component; this is possible because the latter should be symmetric with respect to solar zenith angle and the former will depend strongly on the direction of the solar wind convection electric field (which can be inferred from MAG measurements of the IMF). Next, the bound and unbound components of the sputtered corona can be separated using forward models of sputtering production. In this way, sputtering loss will be characterized as a function of EUV flux, solar wind pressure and IMF direction.

Ion Escape Unlike neutral escape, escaping ions will be measured directly, by the STATIC instrument. This will be done primarily by measuring the flux of ions passing through a planar or hemispherical surface downstream from Mars, and using global models of ion escape for interpolation across locations not sampled by the MAVEN spacecraft. Ion escape patterns will be organized according to Mars-solar-electric field (MSE) coordinates. Our coverage is such that ~ 50 % of the escaping ion flux in the Martian magnetotail can be sampled in as little as 6 weeks. Figure 20 shows an example of the MAVEN orbital coverage in MSE coordinates at a distance of 0.4 Mars radii down the magnetotail from the planet as a function of time. This kind of coverage will allow global estimates of ion escape rates to be calculated for different solar wind pressures and solar EUV fluxes and enable ion loss extrapolation backwards in time (see next section).

STATIC data will also enable us to determine the relative contributions of pickup ion loss, ion outflow and bulk ion escape. The spatial distribution of escaping ions will be measured, including their fluxes, masses, and velocities. Additionally, MAG will measure the background vector magnetic field and the conditions for which escaping ions were measured. This information can then be compared with models to determine the source of the ions (i.e., whether they were picked up as newly created ions in the Martian exosphere).

Similarly, STATIC data taken near and below the exobase region will be able to isolate cold ionospheric ions accelerated outward. MAVEN instruments will measure the ion flows, their composition and the thermal state and density of the ions and electrons as well as the magnetic field that orders the geometry of ionized particle trajectories.

Lastly, MAVEN will make relevant measurements in the ionosphere to assess the importance of bulk ion escape as an atmospheric loss process. Magnetic field, electron velocity and ion velocity and composition data will determine whether the spacecraft is in a vortex-like plasma instability or a reconnection exhaust region indicative of bulk ion loss. The velocity of large-scale flux-rope-like structures previously identified downstream from strong crustal fields at Mars (Brain et al. 2010) can be used to determine whether they are propagating away from the planet (resulting in loss).

Global models of the Mars upper atmosphere and solar-wind interaction are important to reaching MAVEN goals because they allow a large-scale and large-scope integration of results that would otherwise be impossible to obtain because of the limited coverage from the observations alone. Physical models of the Mars upper atmosphere and near-space environment are required in order to interpolate measurements of atmospheric conditions and escape across gaps in physical space, in time, and in the external-driver parameters (e.g., solar input conditions). This interpolation is necessary in order to properly interpret the MAVEN data. To do this, we will utilize two separate coupled three-model frameworks, one from the University of Michigan and one from the Laboratoire de Météorologie Dynamique (LMD) in France. Both frameworks couple a general circulation model (GCM) of the troposphere, mesosphere, thermosphere and photochemical ionosphere upward to a Direct Simulation Monte Carlo (DSMC) model of the neutral upper thermosphere and exosphere, including the transition region from collisional to collisionless physics. Both of these models are used as input to global plasma models of the Mars-solar wind interaction. The Michigan framework uses a global multi-fluid MHD model while the LMD framework uses a hybrid model where ions and electrons are treated kinetically and in the fluid regime, respectively. These models are described in detail in Lillis et al. (2014).

An ever-expanding "model library" will be maintained by the MAVEN project, covering combinations of subsolar longitudes, seasons, solar-wind pressures and IMF directions, for use in interpreting MAVEN data and enabling estimates of global atmospheric escape.

6.4 Goal 3: Determine the Integrated Loss of Atmosphere from Mars over Solar System History

Goal 3 will be approached from three complementary directions: we will extrapolate escape processes backward in time to early solar system conditions to estimate total integrated escape quantities; we will use direct measurements of escape rates at different conditions to allow extrapolation of escape rates back in time; and we will also use measurements of relative concentrations of isotopes and models of isotope-specific escape rates to estimate what fraction of the various gases has escaped over Martian history.

Extrapolation of Processes Back in Time Determining total integrated atmospheric loss to space from measuring loss today will only be possible when we have made substantial progress on goal 2. That is, we first require a reasonably confident understanding of how neutral and ion escape rates at the current epoch vary with the main external drivers—solar wind pressure, EUV flux and SEP flux—all of which are expected to have been greater early in solar-system history. An example is EUV flux, which may vary by a factor of 2 over the nominal MAVEN mission but which is expected to have been up to 6 times higher 3.5 b.y.a. according to models and observations of the evolution of G2-type stars like our sun (Zahnle and Walker 1982; Ribas et al. 2005).

This extrapolation of our multidimensional parameterization of global escape rates will be guided by models of the sun-Mars interaction under such extreme conditions. We can run the models for early-solar-system conditions using different boundary conditions (e.g., with a thicker atmosphere). In this way, we can iteratively "add back" atmosphere through time so our estimates of total escape are self-consistent.

If atmospheric escape rates have a substantial dependence upon Mars' subsolar latitude (and, through that, the diurnally averaged position of the crustal fields with respect to the solar wind), then our iterative modeling backwards in time will have to take account of the large variations in obliquity over Martian history. Average obliquity over the last 5 million years is 37°, compared with 25.2° today. Obliquities for specific times are known only for periods less than $\sim$ 10 million years ago (Laskar et al. 2004), necessitating a statistical model of obliquity-related escape variations.

Extrapolation of Escape Rates If we measure the escape rates today at a sufficiently broad range of solar EUV and solar-wind energetic inputs, we can use the results to extrapolate directly to earlier conditions. The solar EUV, the solar-wind, and solar energetic particle fluxes were greater and more intense early in Martian history. The variability of these properties through time is estimated based on telescopic observations of solar-type stars (Ribas 2010). If we observe sufficiently large excursions from average behavior, and the upper-atmospheric response to them, we can use this to inform extrapolations to early conditions. This extrapolation will gloss over significant issues, such as the varying atmospheric thickness and composition over time, but still will allow a first-order estimate of loss rates under different conditions.

Isotopic Analysis As described earlier, the rates of removal from the top of the atmosphere depend on atomic or molecular mass, so the removal rates differ for the different isotopes of the light stable gases. Escape to space preferentially removes the lighter isotopes, so that a greater degree of loss results in the remaining gas having a higher ratio between the heavier and the lighter isotopes. We can use these ratios to determine the degree of loss of each atom. In particular, we can use the ratios of D/H, $^{13}C/^{12}C$, $^{18}O/^{16}O$, $^{15}N/^{14}N$, $^{22}Ne/^{20}Ne$, and $^{38}Ar/^{36}Ar$ as strong indicators of loss to space. By measuring these ratios at the top of the well-mixed lower atmosphere and at the exobase from where escape occurs, we can derive a nearly model-independent relationship between the measured ratio and the fraction of that gas that has been lost to space. As most of these atoms come from the climate-related gases, and the argon isotopes are an excellent indicator of loss by physical (i.e., not chemical or photochemical) processes, we can derive the net loss of each to space.

Overall The combination of three independent mechanisms for deriving loss to space provides a powerful approach to understanding the loss over time. While each has its advantages and disadvantages and its inherent assumptions, using all three allows us to get a broad understanding of the degree of loss to space and the significance of the role played by loss processes in the history of the atmosphere through time.

6.5 Connections with Other Missions

MAVEN will join a substantial fleet of spacecraft already in orbit and on the surface at Mars, and others capable of making relevant measurements from other parts of the solar system. Although MAVEN is the first mission dedicated to understanding the upper atmosphere, interactions with the solar wind and solar energetic inputs, and the role of loss to space, these other spacecraft make measurements that will contribute to this understanding as well. Some of the connections are as follows:

Mars Express Mars Express has been making measurements of the solar wind, the plasma properties, and the atmospheric properties for a decade. We anticipate that the combination of measurements from both spacecraft will provide significant value in understanding aeronomy at Mars and in determining the escape rates through time.

MRO and ODY These spacecraft are making measurements of the composition and structure of the lower atmosphere that provide substantial boundary constraints on the processes within the upper atmosphere. Of particular interest are the dynamical processes that can drive wave heating and mixing of the upper atmosphere and serve as boundary conditions for the dynamical processes in the upper atmosphere. Measurements of water vapor and dust also determine the seasonal cycles that can affect upper-atmosphere composition and loss processes as well as control the loss of water.

Curiosity *MSL* is making two types of measurements that are particularly relevant to MAVEN. The SAM instrument measures the isotopic ratios and gas abundances at the bottom of the atmosphere. These clearly are important for understanding how to use the isotope ratios to derive integrated loss to space. And the RAD instrument is looking at energetic ions that reach the surface; these relate to the energetic ions that MAVEN will be measuring in orbit.

Mars Orbiter Mission (MOM) The Indian MOM mission launched successfully and entered orbit around Mars about two days after MAVEN. It carries instruments that can provide measurements that are complementary to those from MAVEN. These include an ultraviolet photometer, a mass spectrometer, and a camera and infrared-emission instrument that can provide information on the state of the lower atmosphere.

STEREO and ACE These two spacecraft make measurements of the behavior of the Sun, looking from different viewing angles than MAVEN will see. The combined data sets are complementary, providing substantial information on the behavior of solar storms and the solar wind throughout the inner solar system, and determining their impact at Mars.

7 Data Products and Availability

MAVEN Level 2 data products will be archived with the atmospheres and space physics nodes of the Planetary Data System as required by NASA HQ. Data will be deposited with the PDS beginning six months into the primary mission. At that time, the first three months of observations will be made available. At three-month intervals, each successive three months of data will be made available. The total amount of data projected for the one-year primary science mission, including ancillary information, will be between 1–2 TB. Software tools are being developed to allow data analysis, manipulation, comparison between instruments, and visualization, and these will be made available through the PDS as well.

8 Summary

The MAVEN mission fills a long-recognized gap in NASA's plans for exploring Mars, as the first mission devoted to studying the upper atmosphere, interactions with the Sun and solar wind, and the nature of processes leading to escape of gases to space. As MAVEN had a successful launch, cruise, Mars orbit insertion, and transition phase, we expect the data set it provides to drive our understanding of the Martian upper atmosphere and ionosphere for the foreseeable future.

Acknowledgements The MAVEN mission would not have been possible without the incredible dedication, commitment, and experience of the many hundreds of people (of all job classifications) who have worked on MAVEN. To call out a few by name would feel like a disservice to those not mentioned. They each have our incredible gratitude and appreciation for their efforts. In addition, we benefitted tremendously from the strong support from each of our partner organizations. Funding for the MAVEN mission was provided by NASA, with additional funding from CNES.

References

M.H. Acuña et al., Global distribution of crustal magnetization discovered by the Mars global surveyor MAG/ER experiment. Science **284**, 790 (1999). doi:10.1126/science.284.5415.790

M. Acuna et al., Magnetic field of Mars: summary of results from the aerobraking and mapping orbits. J. Geophys. Res. **106**(E10), 23403–23417 (2001)

D.E. Anderson, C.W. Hord, J. Geophys. Res. **76**, 6666 (1971)

L. Andersson, R.E. Ergun, I. Stewart, The combined atmospheric photochemical and ion tracing code: reproducing the Viking Landers result and initial outflow results. Icarus **206**, 120–129 (2010). doi:10.1016/j.icarus.2009.07.009

M. André, A. Yau, Theories and observations of ion energization and outflow in the high latitude magnetosphere. Space Sci. Rev. **80**(1), 27–48 (1997). doi:10.1023/A:1004921619885

D.N. Baker, S.G. Kanekal, X. Li, S.P. Monk, J. Goldstein, J.L. Burch, An extreme distortion of the Van Allen belt arising from the "Halloween" solar storm in 2003. Nature **432**, 878–881 (2004)

V. Baker, *The Channels of Mars* (1982) (University of Texas Press, Austin)

S. Barabash, A. Fedorov, R. Lundin, J.-A. Sauvaud, Martian atmospheric erosion rates. Science **315**(5811), 501–503 (2007). doi:10.1126/science.1134358

J.-L. Bertaux, F. Leblanc, O. Witasse, E. Quemerais, J. Lilensten, S.A. Stern, B. Sandel, O. Korablev, Discovery of an aurora on Mars. Nature **435**(7), 790–794 (2005). doi:10.1038/nature03603

J.P. Bibring, Global mineralogical and aqueous Mars history derived from OMEGA/Mars express data. Science **312**(5772), 400–404 (2006). doi:10.1126/science.1122659

S.W. Bougher, T.E. Cravens, J. Grebowsky, J. Luhmann, The aeronomy of Mars: characterization by MAVEN of the upper atmosphere reservoir that regulates volatile escape. Space Sci. Rev. (2014). doi:10.1007/s11214-014-0053-7

L.H. Brace, Langmuir probe: measurements in the ionosphere, in *AGU Geophysical Monograph 102*, ed. by R. Pfaff (1998)

L.H. Brace, R.F. Theis, W.R. Hoegy, Plasma clouds above the ionopause of Venus and their implications. Planet. Space Sci. **30**, 29–37 (1982). doi:10.1016/0032-0633(82)90069-1

D.A. Brain, A.H. Baker, J. Briggs, J.P. Eastwood, J.S. Halekas, T.D. Phan, Episodic detachment of Martian crustal magnetic fields leading to bulk atmospheric plasma escape. Geophys. Res. Lett. **37**(1), 14108 (2010). doi:10.1029/2010GL043916

D.A. Brain, F. Bagenal, M.H. Acuña, J.E.P. Connerney, Martian magnetic morphology: contributions from the solar wind and crust. J. Geophys. Res. **108**(A), 1424 (2003). doi:10.1029/2002JA009482

D.A. Brain, J.S. Halekas, L.M. Peticolas, R.P. Lin, J.G. Luhmann, D.L. Mitchell, G.T. Delory, S.W. Bougher, M.H. Acuña, H. Rème, On the origin of aurorae on Mars. Geophys. Res. Lett. **33**(1), 01201 (2006). doi:10.1029/2005GL024782

S.H. Brecht, S.A. Ledvina, J.G. Luhmann, The Martian ionospheric loss rates versus solar EUV flux, in *AGU Spring Meeting 2004* (2004). Abstract #SM44A-02

M.H. Carr, *Water on Mars* (Oxford University Press, New York, 1996)

M.S. Chaffin, J.-Y. Chaufray, I. Stewart, F. Montmessin, N.M. Schneider, J.-L. Bertaux, Unexpected variability of Martian hydrogen escape. Geophys. Res. Lett. **41**(2), 314–320 (2014). doi:10.1002/2013GL058578

J.Y. Chaufray, J.L. Bertaux, F. Leblanc, E. Quémerais, Observation of the hydrogen corona with SPICAM on Mars express. Icarus **195**(2), 598–613 (2008). doi:10.1016/j.icarus.2008.01.009

P.A. Cloutier et al., Venus-like interaction of the solar wind with Mars. Geophys. Res. Lett. **26**(1), 2685–2688 (1999). doi:10.1029/1999GL900591

D.H. Crider, J. Espley, D.A. Brain, D.L. Mitchell, J.E.P. Connerney, M.H. Acuña, Mars global surveyor observations of the Halloween 2003 solar superstorm's encounter with Mars. J. Geophys. Res. (2005). doi:10.1029/2004JA010881

S.M. Curry, M. Liemohn, X. Fang, Y. Ma, J. Espley, The influence of production mechanisms on pick-up ion loss at Mars. J. Geophys. Res. **118**(1), 554–569 (2013). doi:10.1029/2012JA017665

E. Dubinin et al., Electric fields within the martian magnetosphere and ion extraction: ASPERA-3 observations. Icarus **182**(2), 337–342 (2006). doi:10.1016/j.icarus.2005.05.022

E. Dubinin, R. Lundin, O. Norberg, N. Pissarenko, Ion acceleration in the Martian tail—PHOBOS observations. J. Geophys. Res. **98**, 3991–3997 (1993). doi:10.1029/92JA02233

J.P. Eastwood, D.A. Brain, J.S. Halekas, J.F. Drake, T.D. Phan, M. Øieroset, D.L. Mitchell, R.P. Lin, M. Acuna, Evidence for collisionless magnetic reconnection at Mars. Geophys. Res. Lett. (2008). doi:10.1029/2007GL032289

N.J.T. Edberg, H. Nilsson, A.O. Williams, M. Lester, S.E. Milan, S.W.H. Cowley, M. Fränz, S. Barabash, Y. Futaana, Pumping out the atmosphere of Mars through solar wind pressure pulses. Geophys. Res. Lett. **37**(3), 03107 (2010). doi:10.1029/2009GL041814

R.C. Elphic, A.I. Ershkovich, On the stability of the ionopause of Venus. J. Geophys. Res. **89**, 997–1002 (1984)

R.E. Ergun, L. Andersson, W.K. Peterson, D. Brain, G.T. Delory, D.L. Mitchell, R.P. Lin, A.W. Yau, Role of plasma waves in Mars' atmospheric loss. Geophys. Res. Lett. **33**(1), 14103 (2006). doi:10.1029/2006GL025785

J.R. Espley, Observations of low-frequency magnetic oscillations in the Martian magnetosheath, magnetic pileup region, and tail. J. Geophys. Res. (2004). doi:10.1029/2003JA010193

J.R. Espley, Low-frequency plasma oscillations at Mars during the October 2003 solar storm. J. Geophys. Res. (2005). doi:10.1029/2004JA010935

X. Fang, M.W. Liemohn, A.F. Nagy, Y. Ma, D.L. De Zeeuw, J.U. Kozyra, T.H. Zurbuchen, Pickup oxygen ion velocity space and spatial distribution around Mars. J. Geophys. Res. **113**(A), 02210 (2008). doi:10.1029/2007JA012736

X. Fang, S.W. Bougher, R.E. Johnson, J.G. Luhmann, Y. Ma, Y.-C. Wang, M.W. Liemohn, The importance of pickup oxygen ion precipitation to the Mars upper atmosphere under extreme solar wind conditions. Geophys. Res. Lett. **40**(10), 1922–1927 (2013). doi:10.1002/grl.50415

C.I. Fassett, J.W. Head, Valley network-fed, open-basin lakes on Mars: distribution and implications for noachian surface and subsurface hydrology. Icarus **198**(1), 37–56 (2008). doi:10.1016/j.icarus.2008.06.016

A. Fedorov et al., Structure of the martian wake. Icarus **182**(2), 329–336 (2006). doi:10.1016/j.icarus.2005.09.021

J.L. Fox, Upper limits to the outflow of ions at Mars: implications for atmospheric evolution. Geophys. Res. Lett. **24**, 2901 (1997). doi:10.1029/97GL52842

J.L. Fox, A.B. Hać, Photochemical escape of oxygen from Mars: a comparison of the exobase approximation to a Monte Carlo method. Icarus **204**(2), 527–544 (2009). doi:10.1016/j.icarus.2009.07.005

Y. Futaana et al., Mars express and Venus express multi-point observations of geoeffective solar flare events in December 2006. Planet. Space Sci. **56**(6), 873–880 (2008). doi:10.1016/j.pss.2007.10.014

S.B. Ganguli, The polar wind. Rev. Geophys. **34**(3), 311–348 (1996). doi:10.1029/96RG00497

J.M. Grebowsky, S.A. Curtis, Venus nightside ionospheric holes—the signatures of parallel electric field acceleration regions. Geophys. Res. Lett. **8**, 1273–1276 (1981). doi:10.1029/GL008i012p01273

M.R.T. Hoke, B.M. Hynek, Roaming zones of precipitation on ancient Mars as recorded in valley networks. J. Geophys. Res. **114**(E), 08002 (2009). doi:10.1029/2008JE003247

M.R.T. Hoke, B.M. Hynek, G.E. Tucker, Formation timescales of large Martian valley networks. Earth Planet. Sci. Lett. **312**(1), 1–12 (2011). doi:10.1016/j.epsl.2011.09.053

B.M. Jakosky, R.M. Haberle, The seasonal behavior of water on Mars, in *Mars*, ed. by H.H. Kieffer, B.M. Jakosky, C.W. Snyder, M.S. Matthews (University of Arizona Press, Tucson, 1992), pp. 969–1016

B.M. Jakosky, J.H. Jones, Evolution of water on Mars. Nature **370**, 328–329 (1994)

B.M. Jakosky, R.O. Pepin, R.E. Johnson, J.L. Fox, Mars atmospheric loss and isotopic fractionation by solar-wind-induced sputtering and photochemical escape. Icarus **111**, 271–288 (1994). doi:10.1006/icar.1994.1145. ISSN 0019-1035

H. Jin, T. Mukai, T. Tanaka, K. Maezawa, Oxygen ions escaping from the dayside Martian upper atmosphere, in *Advances in Space Research*, vol. 27 (2001), pp. 1825–1830

R.E. Johnson, Plasma-induced sputtering of an atmosphere. Space Sci. Rev. **69**(3), 215–253 (1994). doi:10.1007/BF02101697

R.E. Johnson, J.G. Luhmann, Sputter contribution to the atmospheric corona on Mars. J. Geophys. Res. **103**, 3649 (1998). doi:10.1029/97JE03266

J.F. Kasting, CO_2 condensation and the climate of early Mars. Icarus **94**, 1–13 (1991). doi:10.1016/0019-1035(91)90137-I. ISSN 0019-1035

A.M. Krymskii, T.K. Breus, N.F. Ness, M.H. Acuña, J.E.P. Connerney, D.H. Crider, D.L. Mitchell, S.J. Bauer, Structure of the magnetic field fluxes connected with crustal magnetization and topside ionosphere at Mars. J. Geophys. Res. **107**(A), 1245 (2002). doi:10.1029/2001JA000239

H. Lammer, H.I.M. Lichtenegger, C. Kolb, I. Ribas, E.F. Guinan, R. Abart, S.J. Bauer, Loss of water from Mars: implications for the oxidation of the soil. Icarus **165**(1), 9–25 (2003). doi:10.1016/S0019-1035(03)00170-2

J. Laskar, A.C.M. Correia, M. Gastineau, F. Joutel, B. Levrard, P. Robutel, Long term evolution and chaotic diffusion of the insolation quantities of Mars. Icarus **170**(2), 343–364 (2004). doi:10.1016/j.icarus.2004.04.005

F. Leblanc, R.E. Johnson, Role of molecular species in pickup ion sputtering of the Martian atmosphere. J. Geophys. Res., Planets **107**(E), 5010 (2002). doi:10.1029/2000JE001473

F. Leblanc, J.G. Luhmann, R.E. Johnson, E. Chassefiere, Some expected impacts of a solar energetic particle event at Mars. J. Geophys. Res. **107**(A), 1058 (2002). doi:10.1029/2001JA900178

R.J. Lillis, J.H. Engel, D.L. Mitchell, D.A. Brain, R.P. Lin, S.W. Bougher, M.H. Acuña, Probing upper thermospheric neutral densities at Mars using electron reflectometry. Geophys. Res. Lett. **32**(2), 23204 (2005). doi:10.1029/2005GL024337

R.J. Lillis, D.A. Brain, S.W. Bougher, F. Leblanc, J.G. Luhmann, B.M. Jakosky, R. Modolo, J.L. Fox, J. Deighan, X. Fang, Y.-C. Wang, Y. Lee, C. Dong, Y. Ma, T.E. Cravens, L. Andersson, S.M. Curry, N. Schneider, M. Combi, I. Stewart, J. Clarke, J. Grebowsky, D.L. Mitchell, R. Yelle, A.F. Nagy, D. Baker, R.P. Lin, Characterizing atmospheric escape from Mars today and through time with MAVEN. Space Sci. Rev. (2014, in review)

J.G. Luhmann, R.E. Johnson, M.H.G. Zhang, Evolutionary impact of sputtering of the Martian atmosphere by O(+) pickup ions. Geophys. Res. Lett. **19**, 2151–2154 (1992). doi:10.1029/92GL02485. ISSN 0094-8276

J. Luhmann, J.U. Kozyra, Dayside pickup oxygen ion precipitation at Venus and Mars—spatial distributions, energy deposition and consequences. J. Geophys. Res. **96**, 5457–5467 (1991)

R. Lundin et al., Auroral plasma acceleration above Martian magnetic anomalies. Space Sci. Rev. **126**(1), 333–354 (2006a). doi:10.1007/s11214-006-9086-x

R. Lundin et al., Ionospheric plasma acceleration at Mars: ASPERA-3 results. Icarus **182**(2), 308–319 (2006b). doi:10.1016/j.icarus.2005.10.035

R. Lundin, H. Borg, B. Hultqvist, A. Zakharov, R. Pellinen, First measurements of the ionospheric plasma escape from Mars. Nature **341**, 609–612 (1989). doi:10.1038/341609a0. ISSN 0028-0836

P.R. Mahaffy, C.R. Webster, S.K. Atreya, H. Franz, M. Wong, P.G. Conrad, D. Harpold, J.J. Jones, L.A. Leshin, H. Manning, T. Owen, R.O. Pepin, S. Squyres, M. Trainer (MSL Science Team), Abundance and isotopic composition of gases in the martian atmosphere from the Curiosity rover. Science **341**(6143), 263–266 (2013). doi:10.1126/science.1237966

M.C. Malin, K.S. Edgett, Evidence for persistent flow and aqueous sedimentation on early Mars. Science **302**, 1931–1934 (2003)

M.A. Mandell, V.A. Davis, D.L. Cooke, A.T. Wheelock, C.J. Roth, Nascap-2k spacecraft charging code overview. IEEE Trans. Plasma Sci. **34**(5), 2084–2093 (2006)

W.E. McClintock, N.M. Schneider, G.M. Holsclaw, J.T. Clarke, A.C. Hoskins, A.I.F. Stewart, F. Montmessin, R.V. Yelle, J. Deighan, The imaging ultraviolet spectrograph (IUVS) for the MAVEN mission. Space Sci. Rev. (2014). doi:10.1007/s11214-014-0098-7

M.B. McElroy, Mars: an evolving atmosphere. Science **175**(4), 443–445 (1972). doi:10.1126/science.175.4020.443

M.B. McElroy, Y.L. Yung, Oxygen isotopes in the Martian atmosphere: implications for the evolution of volatiles. Planet. Space Sci. **14**, 1107–1113 (1976)

M.B. McElroy, T.Y. Kong, Y.L. Yung, Photochemistry and evolution of Mars' atmosphere—a Viking perspective. J. Geophys. Res. **82**, 4379–4388 (1977). doi:10.1029/JS082i028p04379

D.L. Mitchell, R.P. Lin, C. Mazelle, H. Rème, P.A. Cloutier, J.E.P. Connerney, M.H. Acuña, N.F. Ness, Probing Mars' crustal magnetic field and ionosphere with the MGS electron reflectometer. J. Geophys. Res. **106**(E), 23419–23428 (2001). doi:10.1029/2000JE001435

T. Owen, J.P. Maillard, C. de Bergh, B.L. Lutz, Deuterium on Mars—the abundance of HDO and the value of D/H. Science **240**, 1767–1770 (1988). doi:10.1126/science.240.4860.1767. ISSN 0036-8075

G. Paschmann, S. Haaland, R. Treumann, *Auroral Plasma Physics* (Kluwer Academic, Dordrecht, 2003)

J.B. Pollack, J.F. Kasting, S.M. Richardson, K. Poliakoff, The case for a wet, warm climate on early Mars. NASA Spec. Publ. **71**, 203–224 (1987). doi:10.1016/0019-1035(87)90147-3

R.M. Ramirez, R. Kopparapu, M.E. Zugger, T.D. Robinson, R. Freedman, J.F. Kasting, Warming early Mars with CO_2 and H_2. Nat. Geosci. **7**(1), 59–63 (2014). doi:10.1038/ngeo2000

I. Ribas, The Sun and stars as the primary energy input in planetary atmospheres, in *Solar and Stellar Variability: Impact on Earth and Planets*, vol. 264 (2010), pp. 3–18. doi:10.1017/S1743921309992298

I. Ribas, E.F. Guinan, M. Güdel, M. Audard, Evolution of the solar activity over time and effects on planetary atmospheres. I. High-energy irradiances (1–1700 Å). Astrophys. J. **622**(1), 680–694 (2005). doi:10.1086/427977

S.W. Squyres et al., In situ evidence for an ancient aqueous environment at meridiani planum, Mars. Science **306**(5), 1709–1714 (2004). doi:10.1126/science.1104559

R.A. Urata, O.B. Toon, Simulations of the martian hydrologic cycle with a general circulation model: implications for the ancient martian climate. Icarus **226**(1), 229–250 (2013). doi:10.1016/j.icarus.2013.05.014

C.R. Webster, P.R. Mahaffy, G.J. Flesch, P.B. Niles, J.H. Jones, L.A. Leshin, S.K. Atreya, J.C. Stern, L.E. Christensen, T. Owen, H. Franz, R.O. Pepin, A. Steele (the MSL Science Team), Isotope ratios of H, C, and O in CO_2 and H_2O of the martian atmosphere. Science **341**(6143), 260–263 (2013). doi:10.1126/science.1237961

P. Withers, A review of observed variability in the dayside ionosphere of Mars. Adv. Space Res. **44**(3), 277–307 (2009). doi:10.1016/j.asr.2009.04.027

Y.L. Yung, J.S. Wen, J.P. Pinto, M. Allen, K.K. Pierce, S. Paulson, HDO in the Martian atmosphere—implications for the abundance of crustal water. Icarus **76**(1), 146–159 (1988). doi:10.1016/0019-1035(88)90147-9

K.J. Zahnle, J.C.G. Walker, The evolution of solar ultraviolet luminosity. Rev. Geophys. Space Phys. **20**, 280–292 (1982). doi:10.1029/RG020i002p00280